CHALMERS
UNIVERSITY OF TECHNOLOGY

Stereolithography of Zirconia- Investigations and Considerations

Investigative Study on Printability and Mechanical Properties

Master’s thesis in Materials Chemistry (MPMCN)

Fredrik Börjesson Sandén

Master’s Thesis 2020-02-26

Stereolithography of Zirconia-Investigations and Considerations

Investigative Study on Printability and Mechanical Properties

Master’s thesis in Materials Chemistry (MPMCN)

Fredrik Börjesson Sandén

Department of Chemistry and Chemical Engineering

Division of Inorganic Chemistry

Chalmers University of Technology

Gothenburg Sweden 2020

Stereolithography of Zirconia- Investigations and Considerations
Investigative Study on Printability and Mechanical Properties
Fredrik Börjesson Sandén

Supervisor: Erik Adolfsson, RISE;
Email: *erik.adolfsson@ri.se*
Examiner: Lars Öhrström, Chalmers University of Technology, Associate Professor, Chemistry and Chemical Engineering, Inorganic Chemistry
Email: *ohrstrom@chalmers.se*

Master’s Thesis 2020-02-26
Department of Chemistry and Chemical Engineering
Division of Inorganic Chemistry
Chalmers University of Technology
SE-412 96
Telephone +46 31 772 1000

Abstract

Zirconia is an engineering ceramic with a comparatively high toughness due to its ability to undergo a phase transformation upon cracking. However, as with all ceramics, the conventional production methods enforce certain constraints upon the shapes that can realistically be made from this material.

Stereolithography is an additive manufacturing technique which shows promise for enabling new ceramic components to be produced. This paper investigates the stereolithographic process for printing zirconia components. The ceramic suspension, debinding, sintering and material performance are all investigated, as are considerations for the printing process itself, such as the resulting surface finish and the densities of the printed objects.

Bending bars of zirconia were successfully printed and measured on average 829 MPa in a three-point bend test. The following Weibull Curve showed a clear separation in two regimens: one for the weaker bending bars and one for the higher ones. The surface finish of the printed objects was found to depend on the orientation of the printed object, as well as the angle of any slopes in the object’s shape.

Keywords: Ceramics, Zirconia, Stereolithography, Additive Manufacturing

Acknowledgements

Jag önskar tacka min handledare, Professor Erik Adolfsson på RISE för all hjälp och vägledning han har gett mig under projektets gång. Likaså vill jag tacka min examinator, Professor Lars Öhrström vid Chalmers Tekniska Högskola för hans rådgivning. Jag vill också tacka mina medarbetare på RISE, i synnerhet Ola Lyckfeldt för hanns engagemang som fick mig intresserad av keramiska material, och Monika Cristea för hennes hjälp under arbetet. Slutligen vill jag tacka min familj, utan vars hjälp jag aldrig hade kunnat skriva ett masterarbete.

Tack.

Table of Contents

1

Project introduction

Engineering ceramics tends to have certain properties, such as brittleness, high thermal and electrical resistivity and a resistance chemical attacks, to name a few [1-2]. They thus possess interesting, more or less unique, combinations of properties. They can, however, be difficult to work with, as unlike polymers or metals they typically cannot be melted or forged (though glass is a notable exception) [3]. Traditionally, engineering ceramics are prepared from a powder which is shaped into a green body which is then sintered. However, the green body is typically fragile and imposes limits on the shapes that can be produced [4]. Some typical methods for working with ceramics involve investment casting or extrusion, to name a few. There are many ceramic materials, but an especially interesting one is Yttria Stabilized Zirconia (YSZ). It is a very hard ceramic with a certain toughness due to an ability to resist crack growth thanks to a stress-induced phase change. Today it mostly finds use in the dental industry as crowns or for certain bone implants with its hardness, optical properties and biocompatibility [5]. It also boasts good ionic conductivity, allowing it to be used as an electrolyte in solid fuel cells [6],[7]. It also finds use in optical fibers and cutting tools, for example in ceramic knife blades.

Additive manufacturing, commonly known as 3D printing, is a relatively young manufacturing method which aims to quickly and automatically produce complex shapes. There are a multitude of different methods, but examples include partial melting of powder beds, material jetting, or photopolymerisation of polymers [8-9]. The latter method is called Stereolithography. It functions by spreading a monomer solution out on a transparent pane and then irradiating it with light from underneath the plane. The light induces polymerization of the solution in the irradiated areas (which are determined by the shape of the desired product). The cured parts are lifted away, and new monomer solution is spread over the bottom pane. The process is repeated until one has the desired product [10].

Of the methods presented above, none are directly applicable to ceramics, as they cannot feasibly be melted or photocured. However, a possibility is to mix the ceramic powder with a monomer resin and then cure it in the desired shape with stereolithography. Then one could trap the ceramic in a monomer network to produce a green-body. The polymer network is then burnt away as the ceramic is sintered as normal.

1.2 Project aim

The aim of this project is to successfully produce bending bars of zirconia using stereolithography. These bending bars should be reproducible and hold a quality comparable to conventionally produced zirconia with respect to strength.

1.3 Project Scope

The project will take place at RISE, Mölndal, using the CeraFab 7500 printer available there. The printable monomer mixture, settings for the printer and burn-off/sintering cycle will all be investigated and modified as deemed necessary. Any produced components will also be investigated, especially their surface structure and strength.

1.4 Project Questions

- Which of the monomer mixture, printer settings, debinding and sintering process is the most crucial for the production of the bending bars?
- Which is the optimal monomer mixture?
- Which are the optimal printer settings?
- How is the debinding/sintering done in the gentlest way?

- How can one speed up the debinding/sintering steps?
- Are SEM and interferometry sufficient to investigate the sintered pieces, or are further methods necessary?

2

Background

The following project aims to produce bending bars from zirconia using stereolithography. The following section will introduce zirconia as a material and explain what makes it such an attractive material from an engineering standpoint. After that, the polymerization reaction will be described, followed by the methodology of stereolithography and further handling of ceramic materials in a 3D-printed context. Lastly, the methods of white light interferometry and the Weibull Analysis will be presented.

2.1 Zirconia Applications

Zirconia is a metal oxide with the formula ZrO_2. As it is not organic or a pure metal it is classified as a ceramic material. As a ceramic, it shares quite a few properties with other, similar materials like alumnia (Al_2O_3). An especially notable trait common among ceramics in general is their high resistance to wear and chemical attacks as well as a high thermal stability. This gives them a potential application in, for example, the mining industry where abrasion against gravel and dust is common, potentially in corrosive environments [2]. Zirconia also finds plenty of use as a biomaterial. While it has been discontinued from hip replacements due to being crystallographically unstable, it does, however, still see niche uses in orthopedics as femoral components in total knee replacements. It is also used in dentistry for CAD-CAM machining of dental crowns, bridging structures for full partial dentures, as well as dental implants and abutments for titanium fixtures [12].

Zirconia also finds an application in solid-oxide fuel cells, where its ionic conductivity at elevated temperatures makes it one of the better alternatives today. It is worth noting that while the yttria (Y_2O_3) serves as a method of stabilizing the zirconia structure, it also supplies oxygen vacancies for the fuel cell to function. Therefore, the zirconia used in fuel cells tend to have a high yttria content, of about 10% [3].

Finally, since Zirconia happens to have an elastic modulus and thermal expansion coefficient similar to those of steel [13]. This lets zirconia function as a thermal coating over iron alloys without fear of breaking. Examples include combustor liners and rotor blades. Zirconia coating can increase the operational temperature of the engine with as much as 200°C [14].

2.2 Mechanical Properties

In many respects zirconia is similar to steel; so much so that it has been called ”ceramic steel” in an article for ”Nature” [15]. Ceramic materials all have a few properties and behaviors in common. One important thing to note is that they are highly sensitive to defects and/or cracks, as these result in a stress concentration [3]. It has been shown that the stress concentration at the tip of an elliptical crack can be described as equation (1). An Elliptical

$$\frac{\sigma_m}{\sigma_a} = 2\left(\frac{c}{\rho}\right)^{1/2} \qquad (1)$$

Where σ_m is the maximum stress at the tip of the crack, σ_a is the applied stress, c is half the length of the crack (major axis) and ρ is the radius of the crack tip. The stress at the crack tip is therefore dependent on the size and depth of the crack. Note that this correlation holds for any non-ductile material.

Another property common to ceramics is their brittleness. As opposed to most metals and plastics, ceramics tend to fracture brittlely at ambient temperatures. This means that they behave elastically until a certain threshold, where they fracture completely, without any plastic deformation. Engineering ceramics also tend to have a high hardness. These properties can be traced to their atomic structures. Covalently bonded substances with an interconnected microstructure (exhibited by multiple engineering ceramics, for example by zirconia, silicon carbide or diamond) typically have high hardness and melting temperatures [3]. In fact, due to similar refractive index and light dispersion, stabilized cubic zirconia is the best material for diamond substitutes in jewelry and some optical applications.

2.2.1 Hardness

As with any ceramic materials, the properties of zirconia will vary depending on the microstructure. The properties of ceramics depend heavily on their density, as their brittle nature makes any defects where stress can be concentrated a potential breaking point. Monoclinic zirconia can withstand about 9.2 GPa at 98% density, whereas a 95% dense piece only endures 4.1-5.2 GPa [14]. Yttria-stabilized zirconia consistently shows higher values, with 1.5% yttria resisting 11 MPa. Further yttria content increases the hardness even more, up to about 15 MPa. A study conducted by G. Ya. Akimov et. al reported a Vickers Hardness of 12.6±0.1 GPa for a sample sintered at 1500℃ for 2 h using a powder with 3 mol% yttria produced by Tosoh.

2.2.2 Toughness

The toughness of pure monoclinic zirconia (the form that is stable at ambient temperatures) is difficult to measure. Zirconia is sintered above the tetragonal-to-monoclinic transformation temperature (1170°C), so when cooled the sample will undergo the phase change and the resulting volume change cracks the material. However, porous samples have been tested with a relative density at 92.2± 0.4% the fracture toughness was determined to be 2.06 ± 0.04 MPa $m^{1/2}$. If extrapolated, this would mean 2.6 MPa $m^{1/2}$ for a completely dense sample. However, a 95% dense sample has been found to have 3.7 ± 0.3MPa m $m^{1/2}$. As such, the extrapolation does not seem too accurate in this case. The toughness for cubic zirconia has been tested and different results have been found. One study determined it to 2.8 MPa m $m^{1/2}$ while another reported 1.8 ± 0.2 MPa m $m^{1/2}$ [14]. These results are for pure zirconia. When alloyed with other oxides, particularly Y_2O_3 or MgO, the toughness is increased significantly. G. Ya. Akimo et al. reports of tetragonal/ cubic zirconia stabilized by 3 mol% yttria with a fracture toughness of 13.2 ±0.2 MPa m $m^{1/2}$. This sample was produced by cold isostatic pressing [16]. Roger Morrell writes in the Kirk-Othmer Encyclopedia of Chemical Technology in the chapter about structural ceramic that PSZ can achieve a fracture toughness of 4-8 MPa m $m^{1/2}$, depending on the type and amount of stabilizing oxide [17].

2.2.2.1 Transformation Toughening

Ceramics are brittle materials compared to metals. Therefore, methods for improving their toughness are interesting to make them more widely useable for engineering applications and ease of use. Crack Shielding is a collection of techniques used to change the microstructure of a ceramic in such a way that it reduces the stress at the crack tip. Examples of such techniques are micro cracking or ductile zones. Another approach, relatively unique to zirconia, is called transformation toughening [18]. Zirconia exists in three different crystal structures which are stable in different temperature intervals. At room temperature and up until 1170℃ zirconia adopts a monoclinic phase. Between 1170℃ and 2370℃ it is tetragonal, and finally it is cubic above 2370℃. The transformation between phases results in a volume change. The transformation between the cubic and the tetragonal phase results in a volume change of about 2.3% and the transformation between the tetragonal and monoclinic phase is 4.5% [13]. When used practically, zirconia is often partially stabilized with ~5% yttria (Partially Stabilized Zirconia; PSZ) [19]. In this solid solution the cubic and tetragonal phases are meta stabilized at lower temperatures. However, when cracked the metastability is disrupted and the material reverts to the monoclinic phase. This results in a volume increase, which compresses the crack and inhibits its growth until even more stress is applied. This mechanism gives zirconia a much-improved toughness [9], strength and resistance [17] to thermal shock compared to other ceramic materials. As such, these are the phases most often used when making components out of zirconia, at least within clinical fields [12]. Of course, the properties of the final component will be dependent on

the yttria content. A higher amount of yttria decreases the thermal expansion coefficient of the material. Furthermore, this mechanism to improve the toughness is dependent on the phase transformation from monoclinic to tetragonal crystal phase. Therefore, zirconia experiences a decline of toughness at temperatures above 800-1000℃, as the monoclinic phase is stable at 1170℃. Thus, at higher temperatures the phase change slows down. The particle size likewise matters for the transformation behavior. Smaller particles are more liable to transform at lower temperatures. [17].
The transformation toughening property can also be used in other materials. Zirconia finds use in solid solution with other ceramic materials as to improve their toughness's via the same mechanism. Al_2O_3, TiB_2 and MgO can all be alloyed with zirconia to gain this property. These materials are called zirconia toughened ceramics (ZTC). [14] [17].
Due to the extreme temperatures where tetragonal and cubic zirconia are stable, they have not been extensively studied in their pure forms. However, various stabilized forms, containing varying amounts of tetragonal and/or cubic phase have been studied, as well as the monoclinic phase, which is stable at ambient temperature. [14]. However, production of larger components made of pure zirconia is not possible, as a material that is sintered and then cooled across the stability threshold between the tetragonal and monoclinic crystal phases. The resulting volume change cracks the pure material [17].

2.3 Chemical Characteristics

Zirconia is a chemically resistant material. It is an amphoteric material and so it acts like an acid in the presence of strong bases and a base in the presence of strong acids [20]. Weaker acids and diluted strong acids do not seem to corrode zirconia. A study conducted by Haifeng Xie et al. revealed that neither citric acid, acetic acid or 5% HF degraded the material significantly with respect to the flexural strength, Vickers surface hardness or surface roughness [21]. Metals of the fifth, sixth and seventh groups of the periodic table does not react with zirconia, nor does most molten, neutral salts. It is, however, strongly corroded by molten alkali metals. Likewise, the alkaline earth metals also corrodes zirconia, reducing it. At elevated temperatures (1800℃) and in vacuum, silicon can also reduce it and titanium oxidized in its presence. At high temperatures it can also form zirconium carbide and carbon dioxide in the presence of carbon [20].

2.4 Biological Characteristics

Zirconia has been given notoriety especially as a material for medical implants both as ball heads for hip replacements and for dental implants, where their wear resistance and corrosion resistance are valued properties. Tests have also been conducted in-vivo and suggests that zirconia implants are biocompatible and osteoconductive [22] [5]. For the use in hip implants (femoral heads) zirconia competes with polyethylene implants and other ceramics such as Al_2O_3. The polyethylene alternatives have historically had problems with wear and debris and Al_2O_3 have been shown to crack in certain circumstances. Yttria stabilized tetragonal zirconia has shown to be tougher and less prone to fracture than the alternatives while still not causing much debris. It needs to be stabilized with yttria, lest it undergoes a phase transition which can result in grain pullout or cracking, increasing the surface roughness and the wear [23]. However, this use of zirconia is now almost discontinued as the metastability makes the material susceptible to aging. It still sees use as an additive to Al_2O_3, however. This material is called zirconia toughened alumina. [12] A similar application where yttria stabilized zirconia is often used is for dental restoration. Compared to other ceramics, it has a higher toughness and strength, and an esthetically pleasing appearance makes it an appealing choice [24]. It can also be colored to better match the patient's surrounding teeth.

2.5 Ceramic Powders

Ceramic components, pressed or produced through additive manufacturing, are all based on powders. The characteristics of the powders will greatly impact the properties of the final piece. The following headlines will explain how the powder affects the final piece, and how the powder is handled.

2.5.1 Effects of the Powder

Among the more important characteristics of the powders are its purity, the particle size and particle size distribution, reactivity and polymorphic form. Impurities in the powder can present problems from a chemical standpoint, where it can impact for example conductivity [25]. Impurities present as inclusions also acts as stress concentrators, decreasing tensile strength [3].

From a strength perspective, an ideal ceramic component should be completely dense. There should not be any voids in such a piece. To achieve this, a good control of particle size and size distribution is necessary. Smaller particles have a higher surface-to-volume ratio, and are therefore more reactive, leading to easier sintering. However, a powder with several different sizes makes for easier packing and a less porous green-body. Less porosity means a denser final component [3].

2.5.2 Ball-Milling

In general, the smaller powder particles the better for a ceramic component. In order to break down particles to a desired size or break up particle agglomerates, ball-milling is a popular technique. The method consists of placing the powder (called the charge) in a closed cylindrical container filled with grinding media (often balls, short cylinders or rods). The cylinder then revolves horizontally and the charge tumbles around inside it. One can also add a liquid to the powder to ensure it does not stick to the corners of the milling cylinder, but then the liquid needs to be removed after the milling process is complete. The main issue with ball-milling is the risk of contamination of the powder. The milling environment subjects both the container and the grinding media itself to significant wear which poses a risk for contamination of the powder. This can be remedied by selecting resistant containers for the milling. Very hard containers and media wears slowly, decreasing the contamination. Tungsten carbide (WC) media can be used for this. Depending on the charge, one can also use media of the same material to reduce the problems caused by contamination [3].

2.5.3 Freeze Drying

Another method to obtain a free-flowing powder that does not agglomerate is through freeze-drying. It can also be used to remove the liquid after a wet ball-milling process. The process begins with the suspension to be freeze-dried being sprayed into a bath of liquid nitrogen. The droplets then instantly freeze without any voids in them. The droplets are then dried by sublimation resulting in spherical granules that can easily be crushed to yield a dense ceramic powder. The granule size distribution can be controlled by the rheology of the suspension and the pump speed and air pressure used during the spraying segment [26].

2.6 Additive Manufacturing of Ceramics

Additive Manufacturing (AM, is a collective name for a host of techniques aimed to produce components or shapes in a free-standing manner, without the need for molds or extensive machining after production. Instead, a computer file contains the information needed to produce the desired part in a single process. From the advent of the first AM techniques in the 1980s, there are now multiple possibilities for production of vastly different shapes in many different materials, including ceramics. With the special characteristics of ceramic materials, only certain AM techniques are suitable for them. These can be divided into three types of processing techniques, described below.

2.6.1 Powder Based Additive Manufacturing Techniques

Powder-Based techniques utilize a dry powder bed as their feedstock. Examples of techniques are, for example 3D printing (not to be confused with the concept of AM, which is sometimes referred to as 3D printing). The basis for this technique is that a binder material is sprayed over the powder bed, gluing the bed together in a desired shape. After one layer is done, new powder is applied, and a new layer is glued to the first one. This allows for a great freedom in the produced shape as no support structures are needed. However, resolution and surface finish are typically poor and for ceramic materials the density is often unsatisfactory. As such, extra work after printing is often necessary [7].

Another, somewhat similar method is called Selective Laser Sintering (SLS). It also uses a powder bed, but instead of spraying a binder to produce a component, it uses a laser to solidify the powder and build the component layer-by-layer. This works reasonably well for plastics and metals with (comparatively) low melting points but becomes impractical for ceramics with their high melting/ sintering temperatures. Lasers can achieve those temperatures, but for densification to take place the exposure time potentially needs to be long. Typically, one has to lower the required temperatures by adding binder materials to the powder bed. There is also the issue of ceramic materials typically having a poor resistance to thermal shocks, as the laser blast will rapidly heat and cool the material, often causing cracks. Currently, this method is not very viable for production of ceramic materials, mainly due to defects of the produced parts [7].

2.6.2 Solid Based Techniques

Solid Based techniques are techniques that strives to use solid, larger chunks of material to form a desired component, rather than basic powder. An example of this is Laminated Object Manufacturing (LOM). This method involves cutting thin layers of some materials into a desired shape, stack them on top of one another and fusing them. With ceramic materials, this is typically done with tape-casted laminates that are fused with a combination of binder materials, compression and heating. Issues with the technique is once again surface finish, especially in rounded structures, and a risk of delamination owing to the layered structure. The method also imposes limits on the produced shapes, as support structures cannot easily be built [7]. Fused Deposition Modeling (FDM) is another solid based technique. It is a widely used technique that functions by extruding a heated mass of feedstock in a set shape. The feedstock is supplied as a filament and heated in the printer nozzle. This, naturally, does not work with ceramics, so to print ceramic components with this technique the filaments are prepared with the desired powder and held together with binder material. The printed piece then needs to be debound by heating and sintered. This technique also has problems with the surface finish, especially since there is little direct control over the layer thickness. The extruded material is free to flow and will do so differently on different layers depending on the structure [7].

2.6.3 Slurry Based Techniques

Slurry based techniques all use a liquid feedstock, most commonly a ceramic powder mixed with a binder. Ink-Jet Printing is a method used to manufacture components a few millimeters in size, as anything larger takes a lot of time. The process is conceptually identical to ”classical” printing with ink and paper. A tiny droplet, mere a few picoliters of liquid, containing ceramic (nano) particles is deposited onto a substrate, the liquid is dried away, and another droplet can be added. This understandably is time consuming, and much hinges on the quality and characteristics of the ink. However, the system has reportedly produced ceramic parts with a feature size less than 100 µm. It also has the issues of imposing limits to the printable designs, as support structures cannot be generated, thereby prohibiting overhanging or hollow structures [7].

2.7 Stereolithography

Stereolithography (SL) is thought to be the most used additive manufacturing technique and studies are ongoing for it to work for ceramics. The system has been reliably used to print objects from Al_2O_3, and this work investigates its use in printing Zirconia. Due to its importance in this work, it is discussed further than the other techniques. The following few headlines will introduce the fundaments of stereolithography and explain why it, of all AM techniques is used for ceramic materials. The production chain of a ceramic component made with SL will also be presented.

2.7.1 The Stereolithography Method

SL is a wet technique. That is, the printed media is a liquid, often a photo curable monomer slurry. It is loaded into a vat and spread to a thin layer with a wiper blade. The manufacturing takes place on a building platform that hangs over the vat. The platform is lowered into the vat and dips into the thin layer of slurry. Then, depending on the information defined in the STL-file, the machine generates the image to be projected onto the building platform. The slurry underneath the building platform is then irradiated with UV-light which induces a polymerization reaction in the slurry, forming one solid layer of polymers and adhering it to the building platform. The platform is raised from the slurry and new liquid is spread with the wiper blade. The process then continues like this, building the component layer by layer, using ”slices” defined in a so-called STL-file.

There are different methods for generating the image that is to be irradiated for every layer. One method is to use a mirror array to generate every layer. This setup is called a Digital Mircomirror Device (DMD) and is the technique used in the Lithoz CeraFab7500 system [27]. In that system, the DMD consists of more than two million mirrors that each can be directed individually to create the required image. Another method is the generation of masks that shields parts of the liquid from light exposure, curing only the parts that are exposed. This method requires the generation of a lot of masks which can be accomplished by a liquid crystal display (LCD) as a reconfigurable mask. The idea then is to convert the CAD model into a grayscale, and the suspension is irradiated depending on the intensity of the grayscale. However, poor resolution has made several systems adopt the DMD approach. [28].

2.7.2 Polymerization Reaction

The polymerization method used for SL is radical polymerization, meaning the polymerization happens due to the presence of free radicals which steadily bind one monomer unit after another in a long chain, forming a polymer. These reactions typically result in heavy molecular weight polymers quickly, even if longer reaction times still are needed for good yields. The reaction proceeds in three distinct steps: initiation, propagation and termination of the reaction. In the first step the free radicals are formed. This can be done by adding an initiator to the monomer mixture, which is a molecule that, in certain conditions (heat, exposure to UV-light etc.) produces free radicals. For SL, photo initiators are the most used [29]. Among these, there are two distinct ways to form the radicals, and the initiators are classified as Norrish Type I or Norrish Type II initiators accordingly. Type I initiators often contain benzoyl groups and generate radicals by absorbing a photon. This transforms them into an excited state and the initiator then undergoes a hemolytic cleavage of an α-bond and forms two radical fragments. Norrish Type II initiators also become excited upon absorbing a photon, but rather than a hemolytic cleavage, they will abstract a hydrogen atom from a donor. The donor then becomes a radical capable of starting the polymerization [30].

Following the formation of the free radicals, the reaction proceeds with the propagation step. The details will differ depending on the monomers involved, but for SL multifunctional monomers are commonly used as they can produce cross linked systems which improves adhesion between layers [29]. Acrylate-based monomers make for popular choices, as they can polymerize fast even in room temperature. It is also worth noting that pre-made slurries for additive manufacturing are sold and ready to print. However, they are not necessarily made for mixing with ceramic powder. The polymerization process is depicted in reaction 1.

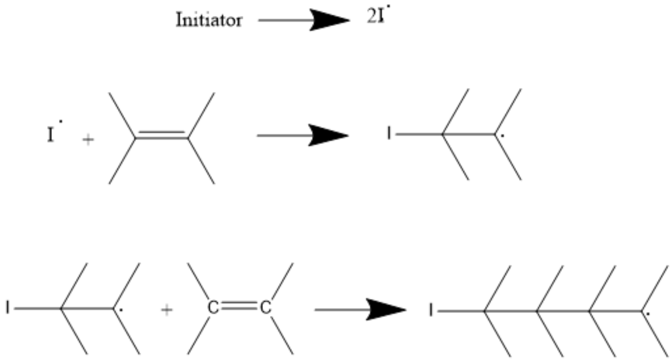

Reaction 1: Initiation and propagation of free radical polymerization

Multiple proposals have been made for how a free radical polymerization terminates, but the prevalent conclusion for polymerization of acrylates seems to be that the polymerization reaction soon becomes diffusion dependent. As the reaction proceeds, the availability of monomers rapidly decreases, and the reaction becomes infinitely slow when there are no more monomers to add to the chain [31]. The polymerization is then considered complete.

2.8 Stereolithography of Ceramics

Based on the procedure described in the previous section, the SL is not directly applicable to ceramics, as they are not liquids anywhere near ambient temperatures, nor are they hardened by UV-light. As such, SL of ceramic components must be done by mixing a ceramic powder with a photopolymerizable monomer. The suspension is printed as normal and the product is then heated in a kiln as to burn away the monomer matrix. In theory this should then leave a green body equivalent of one produced by any ”normal” processing method. The green body is then sintered to full density. There are several parameters that must be handled with care for this system to function. The suspension of polymers and ceramic powder, its contents, rheology and interaction with the UV-light will all impact the printability and result. If the suspension is properly printed, the following debinding- and sintering steps, where the monomer matrix is removed, and the green body sintered to full density can also cause problems [32].

2.8.1 Considerations for the Powder- Monomer Suspension

Ceramic SL requires a monomer mixture with ceramic powder suspended in it to be printed. Ideally the final green body should have a high content of ceramic powder, as to make sintering easier and the final density high. About 50-65% ceramic powder is desirable. The viscosity should be low enough to be easily printable without jamming the machine, but high enough to cover the vat with an even layer for a long enough time to be printed. The viscosity of the pure monomer mixture is very important, as the viscosity increases upon addition of ceramic powder. A less viscous monomer can therefore contain a higher solid loading. To a degree, the viscosity of the monomer mixture can be decreased by addition of a diluent. This is a compound that does not form part of the polymer network itself, but rather takes up space to fill out the network. Addition of such compounds decreases the viscosity and cost of the monomer mixture. Furthermore, since the system is based on irradiation with UV-light, interaction between the mixture and the light must be considered. This consideration takes the form of two parameters: cure depth and light scattering. Cure depth is the depth of the suspension in which the irradiation induces the polymerization reaction. This range needs to be long enough to adhere the newly printed layer to the previous one.

Ideally, the monomer mixture, without any powder, is transparent to the UV-light. However, with powder the suspension becomes turbid and the light can be scattered. This limits the cure depth, and decreases the resolution of the printed component, as the scattered light induces polymerization outside the irradiated area [32].

2.8.2 Component Washing and Debinding

The printed body will be a ceramic powder caught in a polymer matrix. Since no pressure has been applied to the body, the powder is only held together by the polymer matrix, unlike with a normal green-body. Following the printing, the printed body is washed to get rid of uncured suspension clinging to it. This is potentially important as Chang-Jun Bae and John W. Halloran postulates that the uncured suspension might otherwise cure during the debinding phase, leading to mechanical strains in the component, increasing the risk of cracking [33]. The washing should be done gently, as any defects introduced in the body at this stage will remain after it has been sintered [34]. After washing, the polymer matrix must be removed by heat treatment. This step is of utmost importance, as a failed debinding procedure can crack the component. The early part of the debinding process is suspected to require extra caution as the pyrolysis of the polymer matrix and evaporation of the diluent can build up an internal gas pressure inside the component, leading to fractures. The shape of the component is also important. A high surface to volume ratio is beneficial. Debinding of bulky components are more prone to fractures than thin and porous components [18].

2.9 The Sintering Process

Sintering is the process where the powder body (called the green-body) is densified to a solid component. This can be done in a few different ways, but all of them requires some mechanism for material transport and energy that enables this transport. For solid-state sintering, these are diffusion and heat, respectively. Solid state sintering functions due to the energy difference between particle surfaces and contact points between particles. At the contact points the particles can turn their individual surfaces into a grain boundary, with less energy. This process is called necking. Following this, the necks between the particles will grow, decreasing the porosity of the body and leading to a corresponding shrinkage. The centers of the particles will also move closer to one another. The individual particles eventually become grains in the sintered body. Thermodynamics always seeks to decrease the energy in a chemical system. Grain boundaries are more energetic than the bulk material. As such, the boundaries move so that a larger grain grows while a smaller one is consumed. Smaller grains have a larger surface relative to their volume, hence they are more energetic. After this stage the ceramic piece will mostly be densified, aside from isolated porosities. This porosity can only be removed by diffusion through the grain boundaries and is aided by the moving of the boundaries. However, if the boundaries move to fast the porosities can become stuck inside a grain with no way of escaping, leading to a defect in the final component. [3]

2.9.1 Sintering of Zirconia

Zirconia is commonly sintered in conventional furnaces heated by resistivity, even if there are other methods such as hot pressing. Normal temperatures used are about 1450℃ with holding times of 2-4 hours depending on the temperature. There are also ”speed” sintering protocols which operates at higher (1500-1600℃) temperatures with a 30 min holding time. This is to save time [35]. As the sintering temperature and time impacts the microstructure of the material, it will impact the final properties of the produced ceramic. Exactly how it impacts the mechanical properties, however, is still somewhat unclear. Some studies indicate that grain growth occurs above 1300℃ for 3Y-PSZ (3% yttria partially stabilized zirconia), and 1700℃ shows the largest growth. It was found that the sintering temperature correlated negatively to the flexural strength of the material [36]. However, W.M. Ahmed reports of another study that did not find any statistically significant difference in hardness or flexural strength upon ”significantly increased sintering temperature,” [37]. As such, the results are inconclusive, even if a general span of sintering temperatures can be agreed upon.

2.10 Ceramic Densities

Given the nature of how ceramics are produced from a powder that needs to be densified through sintering, the concept of density has been further subdivided to specify what type of density one refers to in any given situation. The ”classical” definition of density, signifying the weight of a specific volume of completely pure material is called ”crystallographic density”. This is calculated from the weight and volume of a material’s unit cell. However, a bulk piece of ceramic will often contain more than one crystal phase with different crystallographic densities, or they might contain other materials altogether, such as alloys or pores with gases. All of these invalidates the crystallographic density as a practical unit of measurement. As such, the term ”bulk density” is used to refer to the density of a ceramic piece, including defects and alloyed materials. It can be determined by simply dividing the mass with the measured volume if the component has a simple enough geometry to be measured. In other cases, Archimedes’ Principle or other methods can be used to determine the volume. As stated previously, a ceramic piece depends heavily on its density for mechanical properties. A component that contains only its intended content, without any pores or defects whatsoever, has what is called ”theoretical density”. This is a figure to measure a produced piece against to see how the product turned out. The closer to the theoretical density, the less defects the ceramic contains. The theoretical density is calculated from the crystallographic density and the content of every solid phase in the ceramic piece [3].

2.11 White Light Interferometry

Since the printing happens layer-by-layer, the surface finish could potentially be worse on the printed objects than on similar objects produced by conventional methods. White light interferometry is a measurement technique that can be used to characterize solid surfaces of both biological and engineered objects. For the purpose of this work, this technique gives information about the surface roughness of the printed objects [37]. Interferometric measurements are based on the phenomenon of light interference. A beam of light is sent towards a beam splitter, which splits the incoming light into two separate beams. One of them is sent towards a reference surface, and the other is sent towards the sample. Both are reflected and recombined before they are sent towards a detector which measures the irradiance of the recombined light. The two beams will have an optical path difference due to the surface roughness (a ridge in the surface means a shorter optical path than a valley, for instance). The different path lengths give rise to different light interferences at the detector, which can be interpreted for a model of the surface [37]. The principal schematic for an interferometer can be seen in figure 1.

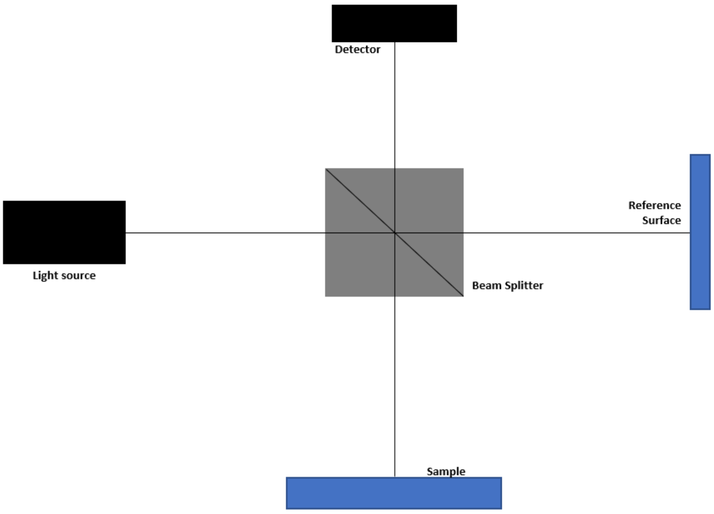

Figure 1 Simple schematic of a white light interferometer.

The results of interferometry measurements are given as abbreviated numbers. For this study, the height of the studied surface (called the Sa number) was used as a measurement of the surface roughness.

2.12 Weibull Modulus

Weibull analysis is a common way to investigate the material properties of ceramics. Due to the nature of these materials being highly dependent on the defect present in each individual sample, a certain degree of chance is involved in their analysis, even under identical testing conditions. To get a measure of this, Weibull statistics can be used. The relation described in equation 2 relates the probability of failure with the strength level of the material [38].

$$P_f = 1 - \exp\left\{-\int_v \left(\frac{\sigma-\sigma_w}{\sigma_0}\right)^m dV\right\} \qquad (2)$$

Where P_f is the probability of failure, V is the volume of the tested specimen, σ_w is the stress level where the probability of failure is zero, σ_0 is the normalized stress and m is the Weibull modulus. The value of the Weibull modulus is a way to determine the variance of the sample strength. A high value on the Weibull modulus indicate that sample strength correlates well to the probability of failure. This, in turn, indicate that flaws in the material are consistent, rather than randomly present or absent. Setting to σ_w zero gives the linear relationship with respect to the Weibull modulus, as seen in equation 3.

$$ln\left(ln\left(\frac{1}{1-P_f}\right)\right) = m\ ln\left(\frac{\sigma}{\sigma_0}\right) \qquad (3)$$

To apply this formula, the tested specimen are ranked in ascending order and a probability for failure is assigned to each one. For this work the that estimation was taken as number of the specific measurement divided by the number of total measurements. Using the probability and the stress at failure for each sample, equation 3 can be plotted and the Weibull modulus is the slope of the curve.

3.

Method

The following headlines will detail the methods used to achieve the results presented. This includes the formulation of the monomer mixture, the powder addition procedure, settings of the CeraFab 7500-9 machine and the debinding/sintering cycle. The analysis methods are also presented

3.1 Monomer Mixture Preparation

The first step of the methodology is the preparation of the monomer mixture. It contains five components: A photo initiator, two different acrylates for monomers, a diluent, and a dispersant. The monomers were chosen as they are compatible with the initiator, and they have different viscosities enabling for easy manipulation of the mixture viscosity. The dispersant was a cationic polymeric dispersant.

The mixtures were made by adding the polymers together in a glass beaker, followed by the diluent, and then the initiator. The mixture was then heated to about 50°C and stirred with a magnet. The heating continued until the initiator (a powder) had dissolved whereupon the dispersant was added, still under heating and stirring. Note that the dispersant is calculated depending on the powder loading. Throughout the project the dispersant was calculated based on a 50 vol% powder loading, but only rarely could that much powder be added without increasing the suspension viscosity to a point where printing was compromised. As such, a little extra dispersant was commonly used in the monomer mixture. Once the dispersant had dissolved, the monomer mixture was removed from heating and stirring, and the powder was added.

3.1.1 Powder addition

The powder is an S-Grade powder manufactured by Tosoh. Aside from the ZrO_2, the powder contains 5.2±0.5 wt% Y_2O_3 [19]. The particle size is 90 nm and the specific surface area is 7± 2 m^2/g. The mixing is performed by deciding on a final volume for the monomer/powder suspension. The aim is always to have 50% powder by volume. The monomer mixture is added to a beaker with external cooling. The beaker is then placed under a stirrer and powder is added in portions while observing the power required by the stirrer to maintain a constant agitation. The power requirement is dependent on the viscosity of the suspension, so this way one can prevent the suspension from becoming too viscous.

3.1.2 Cure Depth Curve

After the powder has been added, the slurry can be printed. However, first a fitting intensity and/or exposure time of the UV-light must be determined. If they are too low, then the suspension will not cure, and printing will be impossible. Too high exposure on the other hand will result in over-curing of the slurry, decreasing the accuracy of the printed component. A fitting exposure time/intensity is determined by slathering some slurry on a microscopy slide and then expose it to a certain light intensity for different times. This will cure the slurry in the exposed area to a certain depth depending on the exposure time. The thickness of the cured slurry layer is then measured with calipers. This also assists in detecting over-curing, which can easily be seen with the naked eye, see figure 2 for an example. The results are plotted, and the resulting curve can be used to determine what exposure time yields a certain cure depth for a certain light intensity and slurry composition.

Figure 2: Two samples for investigating overcuring. Notice the imperfection around the right sample. It has been overcured.

3.2 Printing of the Mixture

A machine from Lithoz GmbH, model CeraFab 7500-9 was used to print all mixtures. The suspension is irradiated with a resolution of 1920x1080 pixels and a 40x40 um plane. The machine consists of a building platform (measuring 78x 43 mm) with an adjustable height above a circular, rotatable vat with a diameter of 16 cm and a depth of 2 cm. The light used to cure the monomers has a constant wavelength of 460 nm. Before the suspension is printed the machine offers a multitude of different settings, presented in table 1.

Table 1. Different settings for the CeraFab 7500-9.

Printer Setting	Range	Typical Setting
Layer Thickness	25-100 µm	25 µm
Wall Thickness Support Structures	250-750 µm	300 µm
Backlight Exposure	0.5-7.5 s	4 s
Exposure Time Start	1-60 s	3 s
Exposure Time General	1-20 s	3 s
Exposure Intensity Start	10-100%	100%
Exposure Intensity General	10-100%	100%
Number of Starting layers	0-2000	5
Shrinkage Compensation (X)	0.1-2	1
Shrinkage Compensation (Y)	0.1-2	1
Shrinkage Compensation (Z)	0.1-2	1
Full Projector Intensity	1-2150	1600
Waiting Times		
Waiting Time Backlight Exposure	5-600 s	120 s
Waiting Time Exposure Start	5-240 s	30 s

Waiting Time Exposure General	0-50 s	16 s
Velocities		
Tilting Down Start	1-30 steps/s	10 steps/s
Tilting Down General	1-50 steps/s	20 steps/s
Tilting Up Start	1-30 steps/s	10 steps/s
Tilting Up General	1-50 steps/s	20 steps/s
Rotation Speed General	10-250 steps/s	100 steps/s
Moving Distances		
Rotation Angle Start	0-1800°	360 °
Rotation Angle General	0-1800°	360 °

Once the settings are in place, the printing can begin. The suspension is loaded into vat and spread to a thin, even layer with the help of a fixed wiper blade. The building platform is then lowered into the vat and irradiated with UV-light from above. This is to secure a layer of cured suspension to the building platform. This layer will act as a base for the rest of the building project. The vat tilts slowly downwards to help detach the printed layer from the bottom of the vat. The building platform is then heightened again, and the vat tilts back up. Then the vat rotates a few times to ensure a good cover of the suspension. The building platform is lowered again, and the first layer of the building project is irradiated and printed onto the building platform. In principle, the system continues the same way until the project is completed.

3.3 Washing of the Component

Once the printing is completed, the printed component is removed from the building platform using a razor blade and washed with Lithosol 20, a compound designed to clean additive manufactured ceramic components. This is to remove any uncured suspension still clinging to the printed piece. The washing is done with a soft brush to gently remove the extra suspension, whereupon the washed piece is dried with compressed air.

3.4 Debinding and Sintering

When the component is washed the polymer matrix must be removed and the ceramic sintered to its full density. Both steps are done by heating the component. Zirconia powder is sintered at about 1450℃, which is well above the burn-off temperature for the polymers.

3.4.1 Burn-off Curves

To get a better understanding of how the debinding process proceeds, a series of burn-off curves are collected. A sample of the pure mixture, without any zirconia powder, is placed in a dish and exposed to an intense UV-light, curing it thoroughly. The solid body is then placed in a kiln with a scale connected to the bottom. The kiln is then heated up to 600℃ at a rate of 1 ℃/min. The change in weight is registered by the scale, allowing one to make a graph over the change in weight in relation to temperature. An example of such a burn-off curve is presented in figure 3.

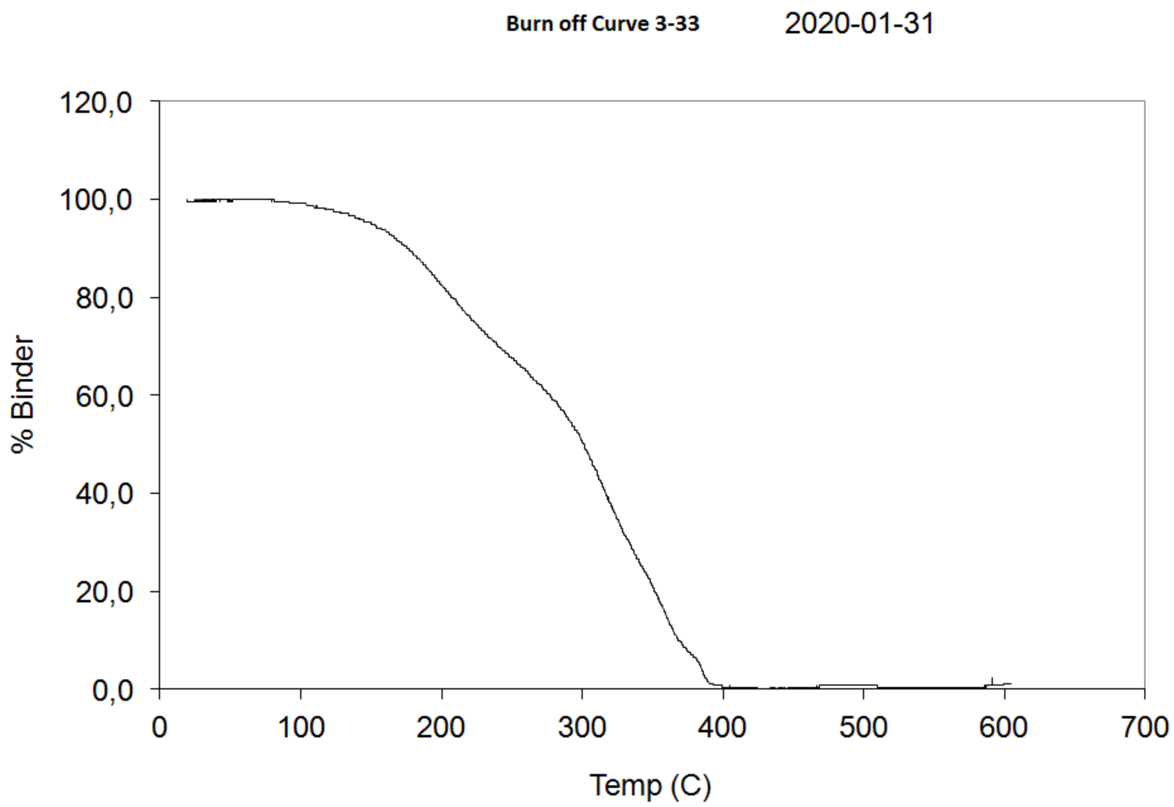

Figure 3: Burn-off curve for mixture 3-33 (without ceramic powder).

3.4.2 Debinding and Sintering Cycle

The burn-off curves for the mixtures are then compared to the curves of the individual mixture components. The comparison reveals that the diluent was lost quickly in the temperature span 200-250℃. This implies that the diluent can become trapped inside the polymer matrix, as figure 3 show only limited weight loss in that temperature range. To avoid a buildup of gasses inside the component, the debinding process had to be slow enough for any gases to escape. A principal debinding process is presented in table 2.

Table 2 A debinding and sintering process.

Process	Temperature Range (C°)	Temperature Change (C°/min)	Time (min)
Heating	0-170	0.1	850
Dwell	170	-	480
Heating	170-250	0.1	800
Dwell	250	-	240
Heating	250-320	0.1	700
Heating	320-600	0.5	560
Cooling	600-0	-	-
Sintering	0-1450	5	290
Dwell	1450	-	120
Cooling	1450-0	5	-

The first heating step is mainly to get rid of extra washing solution. No weight loss was registered at such low temperatures as 170℃. The heating up to 210℃ and the following dwelling time are made to be slow and controlled. As the Diluent should have started to evaporate at this temperature, the kiln remains at 210℃ for 8 hours to slowly drain any gasses that might build up. It is suspected to take a long time, as the polymer matrix remains intact at this temperature. The next heating step, up to 250°C is also slow, as to avoid any sudden release of gasses from inside the component. However, at 250°C the polymer matrix might have started breaking down, opening up the structure. Therefore, the kiln dwells for another four hours at 250°C. The heating from 250°C up to 320°C is where figure 3 predicts most weight will be lost. Therefore, this step is also taken slowly. For the following step, up to 600°C, the kiln is heated considerably faster. At this point there should only be residual organic compounds left, and they should not cause enough disturbance to upset the integrity of the component. At 600°C the component is pre-sintered, to increase durability somewhat. The cooling step is due to a limit in the software used to control the kiln. The software only allows seven steps to be run, and so the script stops after the pre-sintering step. The kiln is then manually restarted, and the component is sintered at 1450°C. The heating can be fast, as there (ideally) should not be any organic components left at this point and the component can be treated like an ordinary, pressed ceramic component. The kiln is held at 1450°C degrees for 2 h to ensure the component is fully sintered, before being gradually cooled down back to room temperature. This is to a voice eventual heat-shocks that could fracture the material during the cooling stage.

Alternative scripts were tested, but the above one was the only one used regularly. An alternative script tested to increase the initial heating ramp considerably, from 0.2°C/min to 0.5°C/min. This was done in the hope that nothing really happened before 170°C, so this would save a lot of time. That time was then used to increase the holding time at 210°C from eight hours to sixteen. Another alternative was to proceed with the old script up to 250°C, and then skip the remaining hold time and slow increase up to 320°C and instead go directly from 250°C to 600°C with a heat increase of 0.5°C/min.

3.5 Component analysis

The sintered components are analyzed in a few different ways. First, they are painted with a marker pencil and washed with ethanol. This removes any exposed color, but leaves any cracks highlighted. The faulty bending bars are then studied with an optical microscope to see how they have cracked.

3.5.1 Determining Density

The density of the component is determined using Archimedes Principle. First the sintered component is marked for ease of recognition and weighted in its dry state. The components are then placed under vacuum for at least 45 min as to remove any absorbed water from their structures and bare any open porosity. After that, the components are submerged in a water bath for at least an hour, still under vacuum. The water bath is periodically shaken as to remove any air bubbles formed on the bottom. This procedure ensures that the water will have plenty of time to diffuse into any open porosity in the piece. After the hour has passed, the entire water basin with the components are moved onto a scale with a hanging platform for weighing the components in the water.

The pieces are weighted while still submerged in the water. Due to the lift of the water being proportional to the volume of the component, this figure is a type of volume measurement. Finally, the pieces are weighted in a" moist" state. That is, they are removed from the water bath and gently wiped with a moist towel. This removes the water droplets on the surface while preserving the water absorbed the ceramic porosity. The moist piece is then weighted. With these three numbers- the dry weight, the wet wright and the moist weight, the bulk density can be calculated from equation 4.

$$\frac{\left(\frac{M_t}{M_f - M_V}\right)}{\rho_{ZrO_2}} \cdot \mathbf{100} \qquad (4)$$

Where M_t is the mass when dry, M_v is the mass when wet and M_f is the mass when moist, and ρ_{ZrO_2} is the crystallographic density of zirconia.

3.5.2 Expansion-Contraction measurement

It was suspected that the bending bars undergo expansions and contractions during their debinding phase. To study this phenomenon, a laser triangulator was rigged up outside a kiln with a slab of isolation and a glass pane for protection against the heat. The slab had a narrow slit to let the laser through, and a hole to collect the reflected light of a standing bending bar. This can be seen schematically in figure 4.

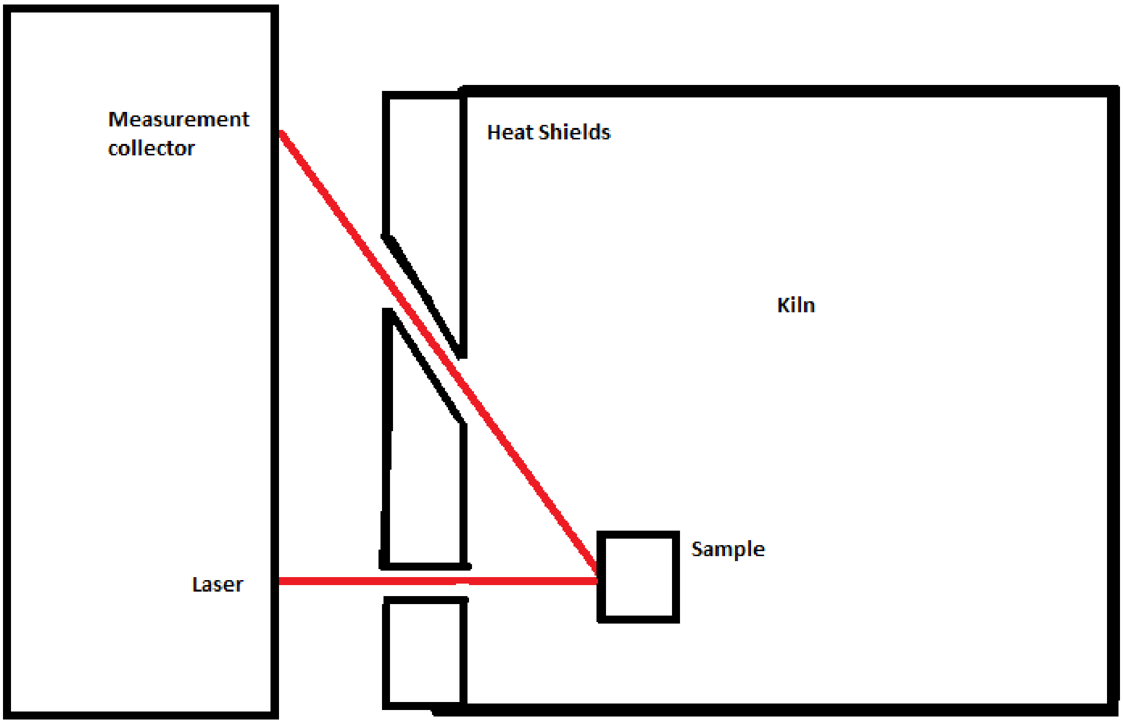

Figure 4: Schematic drawing of the triangulation measurements, as seen from above.

The kiln was then set to change the temperature with 0.1 °C/min and the triangulator measured the height of the bending bar once every hour until the kiln had gone up 350°C and down again to ambient temperature. Following this experiment, a new bending bar was placed in the kiln and the temperature was increased with 0.1 °C/min until the temperature had gone up 170°C, where it was held for about 24 hours. The temperature was then increased to 350°C.

3.5.3 Bending Bar Preparation

The bending bars produced have the dimensions 3.2X3.2X31 mm when printed, and 2.5X2.5X24 mm when sintered. To get a standardized size, one of the short sides must be ground down. The resulting in a bending bar then has the dimensions 2.5X2.0X24 mm. This was done by gluing the printed bars to a plate and cut them with progressively finer grinder wheels. The wheels used diamonds for abrasive. Note that the resulting bending bars are not uniform, as one side has been ground down, while the other retains the texture as printed. Finally, before the bending bars are tested, the long edges on the ground side are dulled. This is to ensure the bending bars rests squarely on the stand during the bend test, rather than on just the corners.

3.5.4 Impact on the density due to sintering temperature

Sintering temperature impacts how the sintering happens. At low temperatures the process is slow, while at high temperatures it is quicker. To investigate how this affects the component density, a set of bending bars were printed, debound and then sintered in different temperatures. The temperatures tested were: 900°C 1300°C, 1350°C, 1400°C, 1450°C and 1500°C. Furthermore, disks of conventionally produced, pressed zirconia was also sintered at each temperature except 900°C to investigate the difference between the production methods. All components were sintered for 2 hours in each temperature.

3.5.5 Three-Point Bend Test

The prepared bending bars were tested in a three-point bend test as to evaluate the material performance. The effective length of the bending bars during the test was 20 mm for all of them, and they were tested with the ground side downwards (that is, the fracture would develop in the ground side and spread upwards towards the printed side).

3.5.6 Different Sized Components

It is suspected that an increased thickness of the printed goods leads to difficulties in the debinding process, as the monomers must diffuse a longer way through the component. To investigate this, components with different thickness were manufactured. These were 8 mm tall and had a thickness of 3.2, 4.2, 5.2 and 6.2 mm (as printed, before debinding and sintering). They were all printed in a vertical fashion and then debound with a standard procedure. Two bending bars scaled 1:2 were also produced (thus having the dimensions 6.4X6.4X62 mm). Furthermore, two hollow cylinders with an outer radius of 20 mm and a wall thickness of 4 mm were produced from suspension exp-33.

3.5.7 Surface Roughness

To determine the surface finish of the printed goods, a series of special components were printed. They were made to have determined angles in relation to the building platform. Due to the layer-by-layer building process, different angles would have a different number of ridges, depending on how steep the sides were. This can be seen in figure 5**.** Three different test components were made. One with the angles 30° and 60°, another with 45°and the final one with 15° and 75°. By how the components were made, there are two of each angle, one being printed with the light coming from underneath the measured surface, and one where it comes from above.

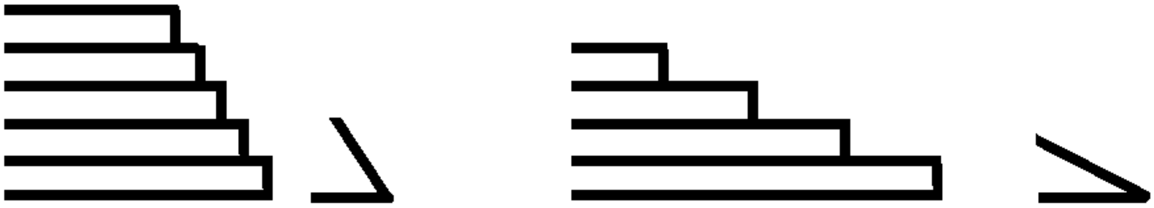

Figure 5: Pictographic representation of how different angles gives different surface roughness.

4.

Results and Discussion

Two recipes for the monomer mixtures were tested during this work. Suspension 3-33 was used to develop the technique and manufacture the bending bars used to evaluate the material performance. The other suspension (called Exp-33) used an alternate recipe and was used to print bulkier components. Throughout this study, it was often difficult to say what part of the method was responsible for a failed component. All but the most obvious flaws can only be discovered after the printed piece has been printed, debound and sintered, and then the flaw often cannot be traced to any particular step in the method. At best one can make educated guesses.

4.1 Results regarding suspension 3-33

The recipe for the monomer mixture used for most of this study was one of many developed previously and is referred to as suspension 3-33. It was selected for further study as it had, of all investigated recipes, the highest content of the more viscous monomer, a comparatively heavy monomer which was suspected to have reduced shrinkage upon debinding, which in turn would prevent stress buildup in the component. Powder content added to the mixture varied between 42vol% and 49vol %, but the latter proved to have such a high viscosity at ambient temperature (here 18 °C) that it was difficult to print. It was also challenging to satisfactory disperse that volume of powder without clogging the dispersion setup. As such, this experiment was never repeated. It did, however, prove the importance of the suspension’s shear-thinning properties. The suspension was subjected to heavy shear during the dispersion of the powder, but once the shear was removed it quickly became much more viscous to the point of being unusable. Less viscous suspensions of about 44-45vol%could be printed, even if much suspension was lost from the process as it stuck to the walls of the vat and stayed there, away from the wiper blade.

Of the standard suspension, containing two types of monomers in a ratio 1/2, and a total of 33vol% diluent, two different contents of initiator was used. One recipe used 1vol% initiator, while the other recipe used 4%. These two suspensions, of course, showed drastic differences in sensitivity towards UV-light. The one with less initiator required longer exposure time as well as stronger light intensity in order to polymerize satisfactory**.** This aside, none of the two mixtures were clearly better than the other with respect to the quality of the printed goods, as they both similar number of successful printing attempts. An example of how cure depth depends on exposure time can be seen in figure 6. Both variants of the initiator showed the same type of logarithmic dependence.

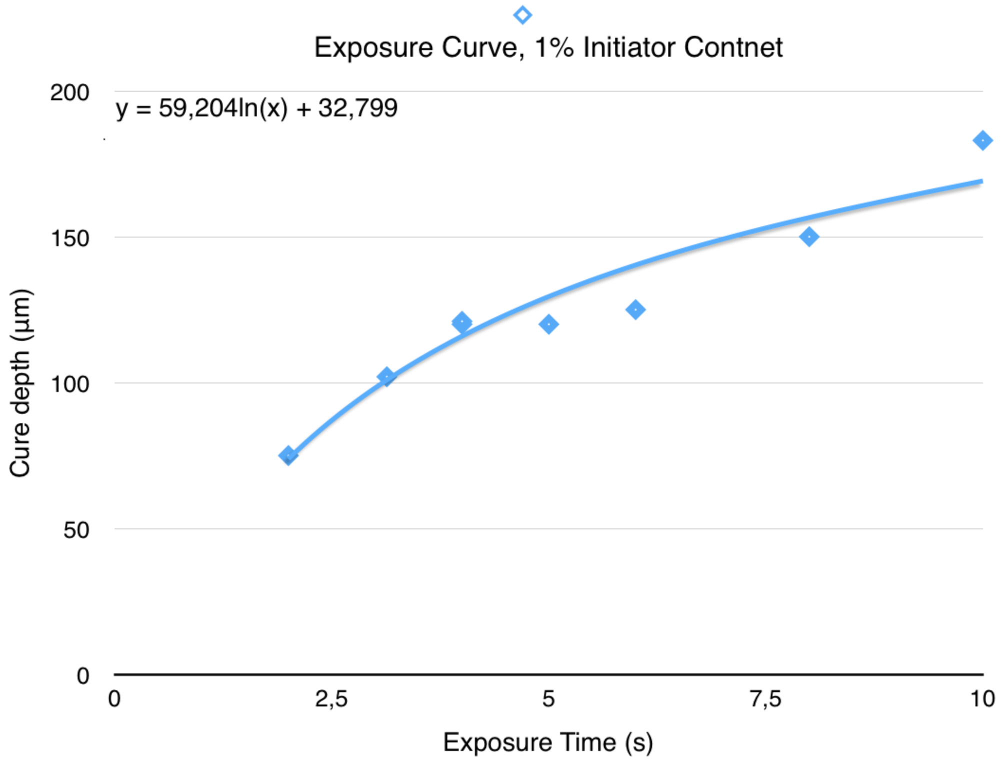

Figure 6: Typical Exposure curve taken at light intensity 1600. This is used to determine cure depth depending on exposure time. It does not say anything about overcuring.

No matter the initiator content, the suspension proved to be highly dependent on temperature. Upon storing the suspension in a warm environment of about 40 °C its viscosity decreased severely. Following this discovery, a small radiator was placed in the printer, bringing the temperature up to 30°C. Following these modifications, suspensions of 46-47vol% zirconia could be routinely printed. The shear thinning effect remained prevalent, but the suspension no longer stuck to the upper parts of the vat in any significant amount, leading to greater suspension economy. The lower viscosity also simplified cleaning. The low viscosity of the suspension easily ran off the printed components during the printing process, rather than clinging to it. This resulted in less suspension having to be cleaned, which further improved the suspension economy. Furthermore, the shelf life of the suspension depended on the viscosity, and consequentially was increased when the suspension was stored warmly.

The suspension of 46-47 vol% zirconia could repeatedly be printed in a heated environment, debound and sintered successfully. This was by far the most common procedure that was used to produce satisfactory goods throughout this work. All the analyzed bending bars were produced from this suspension.

4.2 Results regarding suspension Exp-33

Suspension Exp-33 differs from 3-33 in its ingredients. Exp-33 does not contain any of the viscous monomer at all. This recipe resulted in a much more fluid mixture which, in theory, would allow for a greater portion of powder to be added without viscosity becoming an issue. This, however, was not tested; all batches made of Exp-33 had the same powder content as contemporary batches of 3-33 at about 47vol%. Exp-33 also proved to be notoriously harder to polymerize (at 1 vol% photo initiator content), requiring an exposure of 6 seconds. This is compared to 3-33 with the same photo initiator content, which needs about 3.5 seconds. The goods printed using the Exp-33 suspension is also more flaccid than something printed from regular 3-33. Successfully debinding the bars produced from Exp-33 proved challenging, as the normal debinding script caused catastrophic delamination along the entire length of the bending bars when used. There are currently two hypotheses that might explain the tendency towards delamination during debinding. Either, the cross linking provided by the more viscous monomer is necessary to keep thin objects like bending bars together, or the lack of crosslinks makes it easier for the diluent to leave the polymer network.

4.3 Results regarding positioning of the goods on the printer bottom plate

The bending bars were printed as cuboids with the dimensions 3.2X3.2X31 mm. This allows for two different printing possibilities: either they can be printed with the long side laying down towards the bottom plate or standing with a short side down towards the plate. An example of the latter can be seen in figure 7.

Figure 7: A completed printing process where the bending bars have been printed in a standing fashion.

The positioning of the bars during printing has a major impact on their structure, as the machine prints them layer-by-layer. The standing position bars requires many more layers to complete than the laying bars. Furthermore, when the bending bars are tested in a bend-test, the standing bars will have the force applied in the direction of the layers, while a bar that has been printed in a laying fashion will the force applied perpendicular to the layers. Since a major problem throughout this work was fractures between the layers (delamination), it was assumed that force applied in the same direction might have a strong impact on bending bar performance. Therefore, most of the bending bars were printed in a standing fashion.

4.4 Results regarding the printer settings

Multiple printer settings were tested throughout this work. Especially the hold time between the lowering of the ceramic piece into the vat and the irradiation with UV-light was considered of great importance, as it was suspected air bubbles could become trapped underneath the printed object and captured inside the polymer network. Then it would then remain there and become a defect when sintered. A longer hold time in conjunction with a non-viscous suspension would give the air bubbles

time to escape and improve the quality of the sintered piece. However, the results do not show significant improvements from longer holding times.
The other parameter thought to be important during the printing process was how the printed part was lifted from the vat after irradiation. It was theorized that a careful lifting process would improve adhesion between the layers in the piece, decreasing the risk of delamination, as seen in figure 8**.**

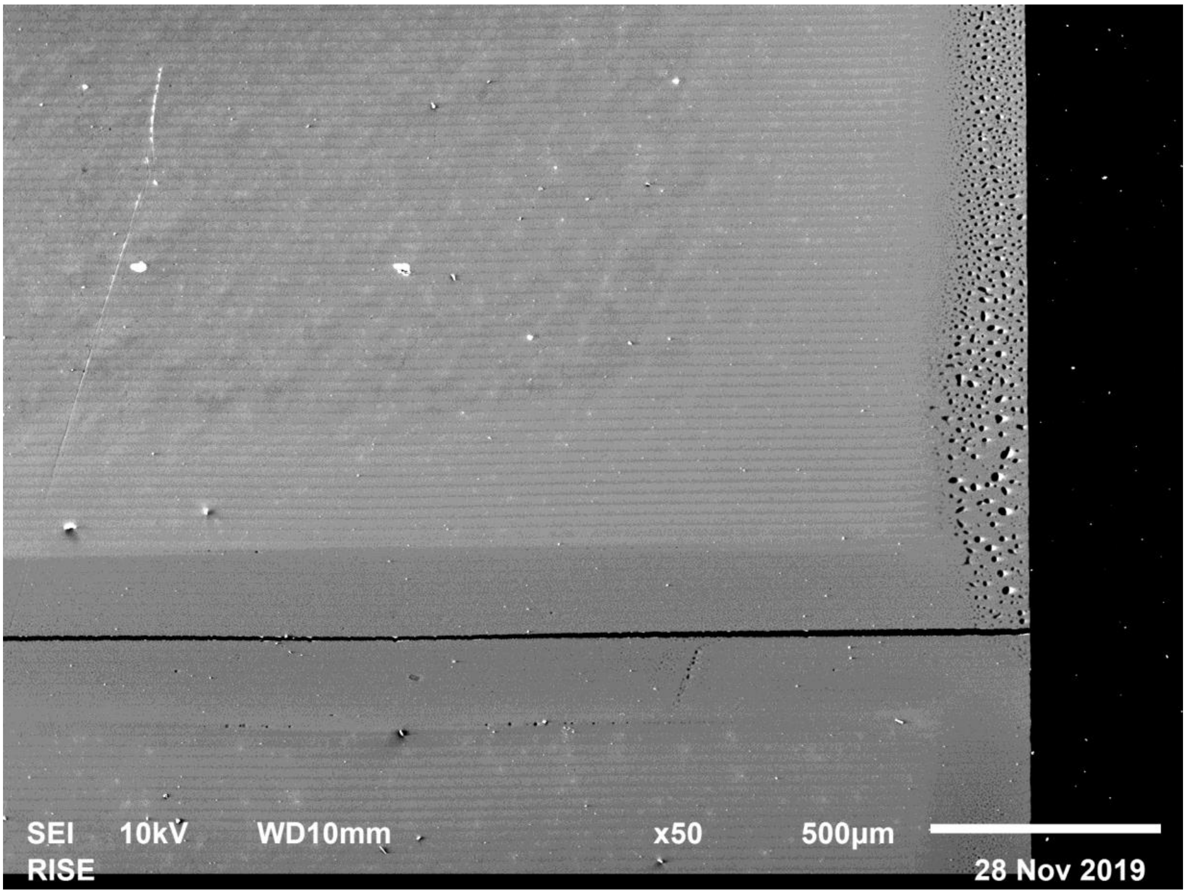

Figure 8: Bending bar that has been heated up to 310 °C. Notice the layered structure, and how the fracture goes exactly through the interface between two layers.

Two changes were made to improve the lifting process. The simplest was to decrease the speed with which the vat tilted down from the printed piece, and the other was to rotate the bending bars so a corner was lifted of the vat first, rather than the entire width of the bending bar at the same. Doing so failed to yield any conclusive results for better or for worse.

4.5 Results regarding the debind Script

The debind script was adapted from a previous work on the same material. This, in conjunction with the burn off curves, gave a debinding script that proved to work from the very beginning; no changes were necessary. Investigating both the burn off curves presented in figure 9, 10 and 11 and the shrinkage during the debinding process, presented in figure 12, revealed that no noticeable weigh loss or shrinkage happens before about 150°C. Then the shrinkage begins and continues up to about 250°C. After that, most of the shrinkage in the debinding step is done. The weight loss proceeds rapidly between 200°C and 300°C, and then decreases up to about 500°C. Luckily, the original debinding script used slow heating up to 320°C which is well above the most critical regions. Alternative scripts were tested, however. One script was tested where the initial heating was done significantly faster, 0.5°C/min instead of 0.2°C/min, and instead the hold time at 210°C was lengthened to sixteen hours. This, however, proved disastrous, as all the bending bars had broken apart completely in the kiln, something that only strengthens the theory that the debinding at low temperatures is a vital part of the debinding process that must be handled with care.

4.5.1 Burnoff Curves

The burnoff curves were made to find out at what temperature and how fast the monomer is removed from the component during debinding. Figure 9 shows the burn off curve with respect to temperature and weight for the pure Exp-33 polymer. That is, the polymer without any ceramic powder added.

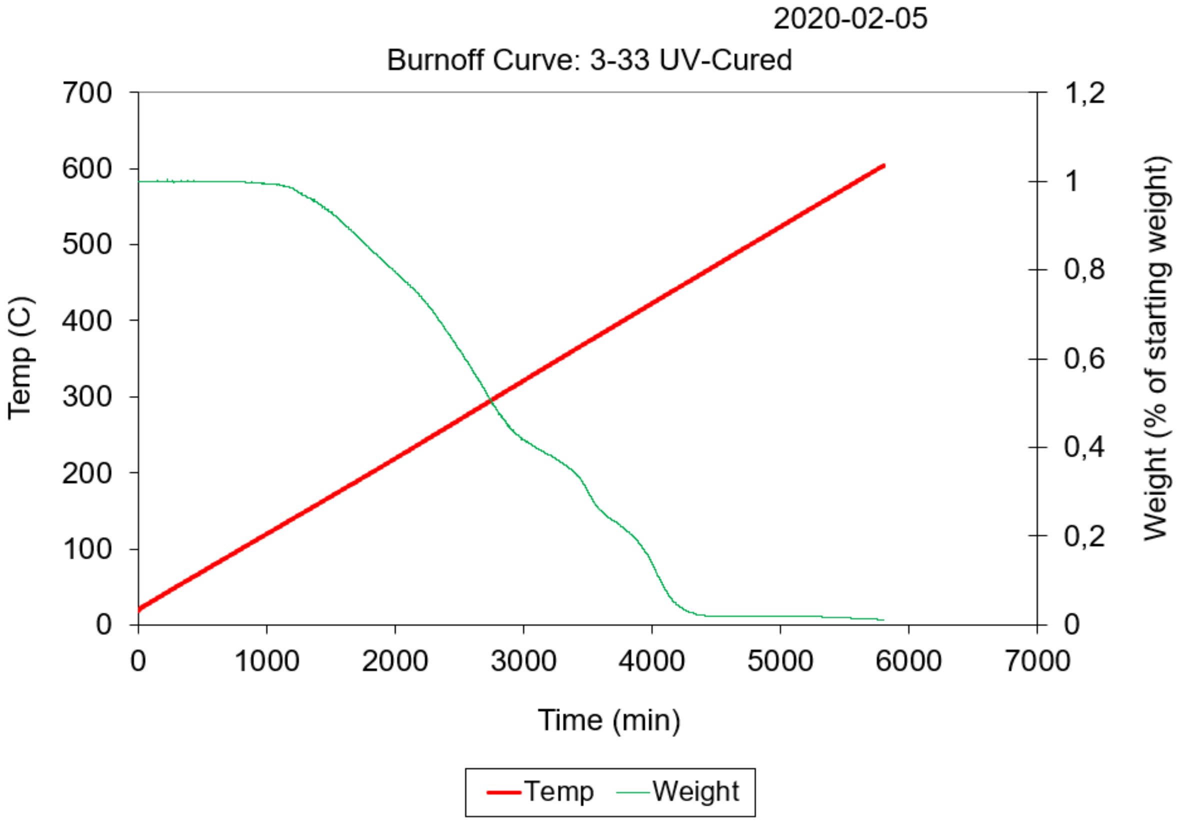

Figure 9: Burnoff Curve for pure 3-33 polymer. The temperature increases with 0.1 °C/min up to 600°C. The experiment ran for about 96 hours. Different, somewhat linear weight loss processes can be seen between about 150- 200°C and 250-300°C.

As seen in the burnoff curve, the weight loss varies a great deal with the temperature. It is suspected that the earliest decrease is due to the diluent evaporating, as it has the lowest boiling point of the components and should not be chemically bound in the polymer network. The next two decreases in mass are most likely due to the two polymers disintegrating at different temperatures in conjunction with diffusion out of the solid polymer cake.
This result can be compared to an experiment conducted on the same polymer system with ceramic powder added.

For this experiment, printed goods were placed in the same kiln and debound with the same temperature increase of 0.1 °C/min. The Burnoff Curve for the first can be seen in figure 10:

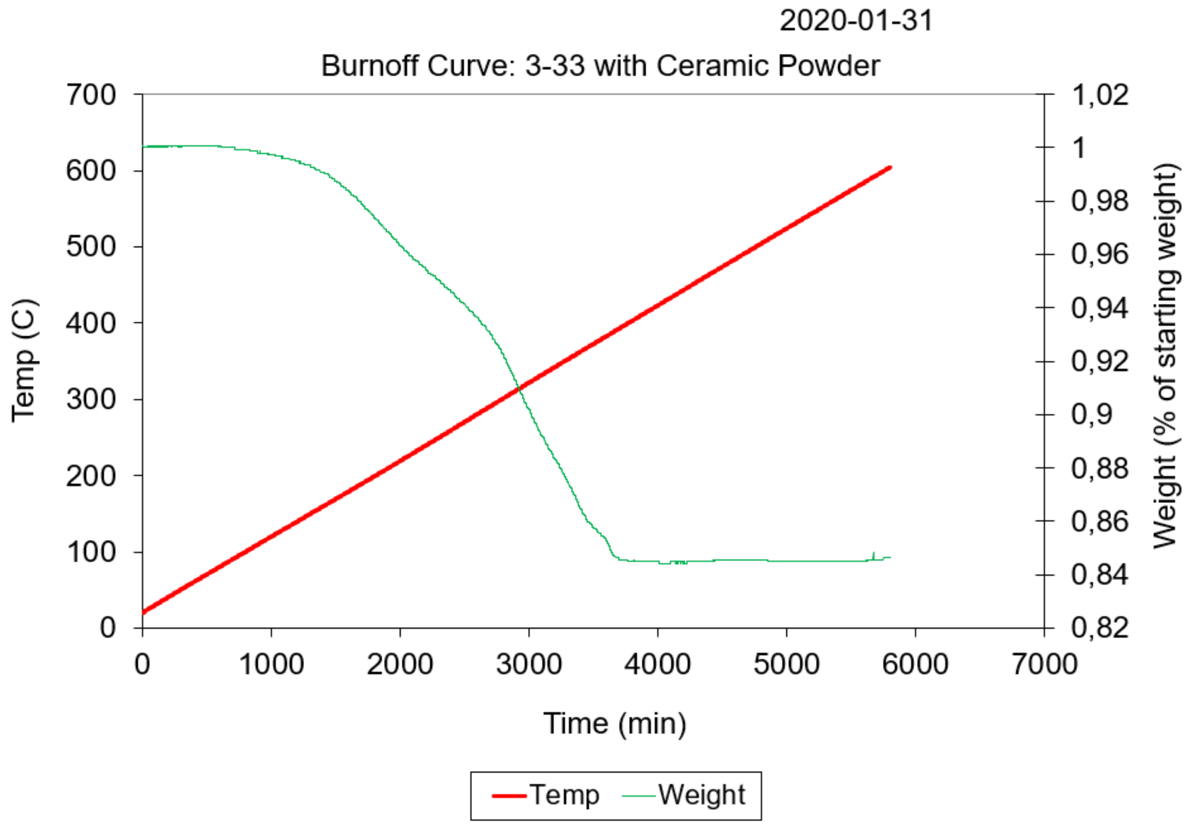

Figure 10: Burnoff Curve for 3-33 polymer- ceramic mixture. The temperature increases with 0.1 ℃/min up to 600 ℃. The experiment ran for about 96 hours. Different weight loss processes can be seen between about 100- 250℃ and 300-350℃.

The curves look largely similar, as the same regimens seems to be present. The main difference is that the curve in figure 9, without the ceramic powder, seems to consist of linear regimens, whereas the other curve has a smoother appearance. This can be attributed to the powder making the diffusion of the polymeric material more difficult, thus slowing the process down. The polymer cannot leave the body even if the temperature is high enough due to the diffusion hindrance. Another noticeable difference between the curves is the sharp decline of the curve depicted in figure number 10 around 250-300℃. No decline as sharp can be seen in the other curve.

The hypothesis regarding this behavior is that the diluent should evaporate before the polymer network itself, in order to open the network and simplify degradation and diffusion of the polymer itself. Therefore, if the powder prevents the diluent from evaporating properly, it will also disrupt the degradation of the polymer network further down the process. This results in the polymers burning away faster once the system is open enough to enable diffusion into the powder body. This result can potentially become important when attempting to print bulkier pieces. Such a piece will be even more hindered on the diffusion. If the temperature rises too fast, then the buildup of gases inside the powder body might lead to an internal pressure, followed by cracks. The issue can be alleviated with isothermal holding times during the debinding, to ensure every component of the monomer mixture can evaporate.

It is worth noting that the weight percentage of the curve depicted in figure 10 never reaches 0. This is because the bulk of the weight is the ceramic powder. The density of the monomer suspension is approximately 1 g/cm^3, whereas for the zirconia powder it is about 6.05 g/cm^3.

4.6 Results regarding the shrinkage during debinding

While the sintering results in a large shrinkage of the printed piece, it was suspected that certain shrinkage also happens as the polymer network is removed during the debinding. The following headlines explore this hypothesis.

4.6.1 Results regarding the contraction during a uniform temperature increase

The triangulation measurement revealed that the bending bars do indeed contract during the debinding step. The logged data can be seen in figure 12.

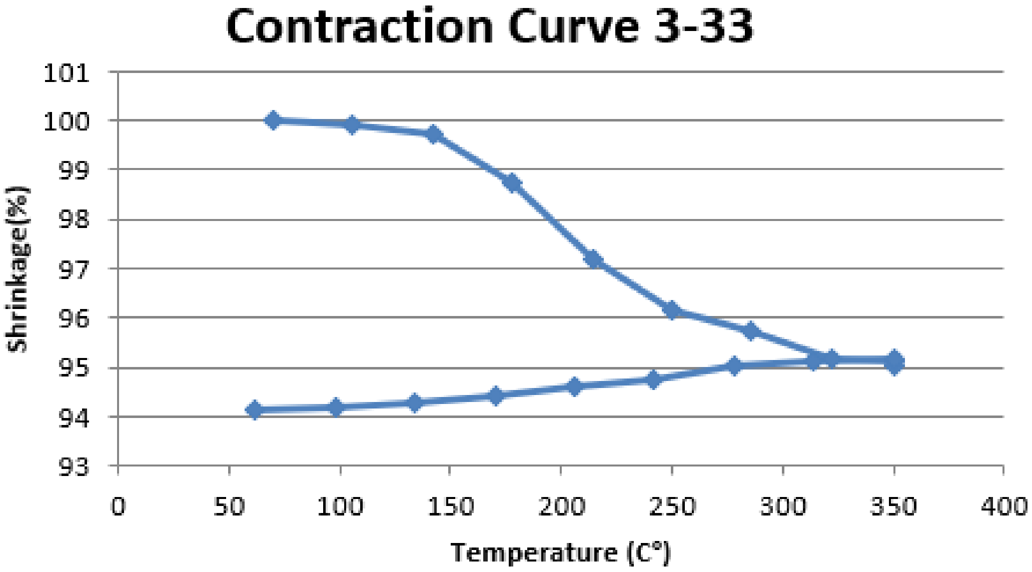

Figure 12: Contraction of the standing bending bar during debinding. Most of the contraction happens early in the process, at temperatures around 200 °C. The temperature increased with 0.1 °C/min for the entire measurement up to 350 °C, and then decreased at the same rate down to about 50 °C.

Most of the shrinkage happens at a temperature of about 150-250 °C. This is also around the temperature where most of the weight loss happens, according to the burn off curves in figure 9, 10 and 11. However, the curve presented in figure 12 are for the suspension containing two monomers (3-33), whereas the burnoff curves presented in section 4.5.1 were for Exp-33- as such, they cannot be directly compared with each other. Their behavior is expected to be relatively similar in the early parts of the debinding procedure, however, as they contain the same amount of diluent which is established to leave first. should be noted that the contraction was measured on a printed piece containing both ceramic powder and polymer, whereas the burn off curve was measured on polymer alone. It therefore stands to reason that the polymer removal process should be easier in the burn off scenario, and yet the shrinkage starts before then. C. Bae and J, W. Halloran postulates that the increased temperature might activate any remaining photo initiator, inducing polymerization during the debinding phase [33]. It is possible that such a procedure could result in further shrinkage of the component. If so, then the shrinkage might be the result of this polymerization first, in the lower temperatures, and then the removal of the polymer network at higher temperatures, where the weight loss can be observed. Possibly these processes could occur in tandem, without any way of differentiating them from one another. There is a slight shrinkage in the cooling process.

Another shrinkage experiment was made where the bending bar had been printed in laying fashion. This was to investigate the difference in shrinkage in different dimensions. A standing bending bar and a laying bending bar would have their individual layers in different directions. The resulting shrinkage curve can be seen in figure 13.

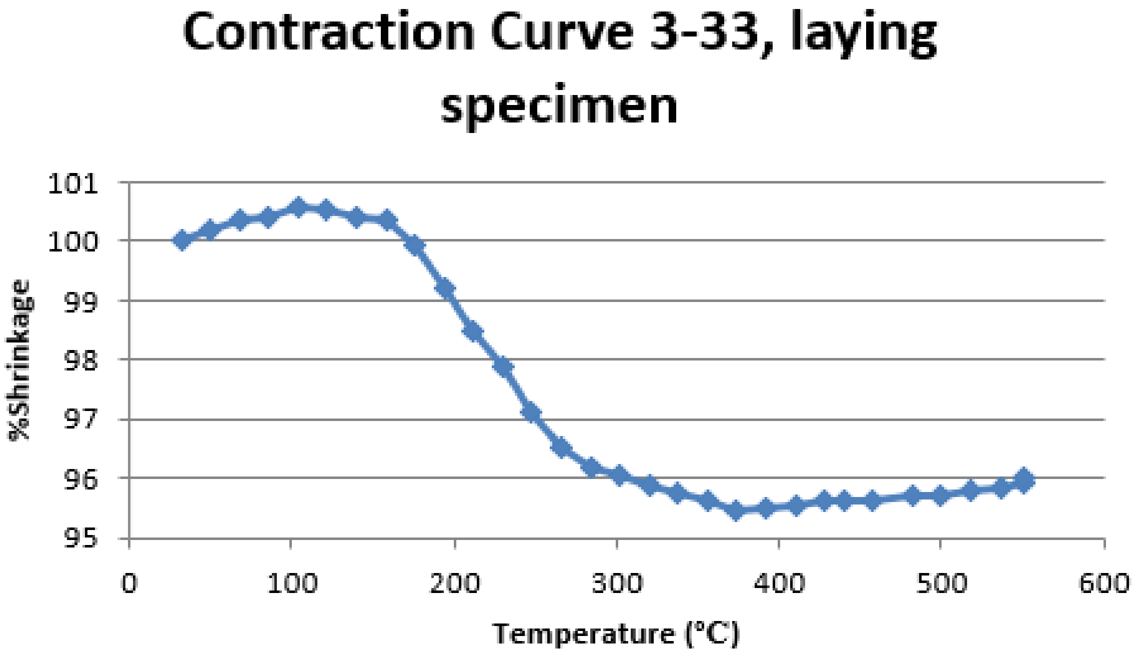

Figure 13: Contraction of the laying bending bar during debinding. Most of the contraction happens early in the process, at temperatures around 200 °C. The temperature increased with 0.1 °C/min for the entire measurement up to 550 °C.

The two processes seem to be similar. The slight increase at the beginning is probably due to a slight expansion of the polymer network upon heating. Most of the cooling happens similarly as with the standing bar, which is to be expected as the processes when underway should be similar. The final results for both processes are a little bit different with the standing bar shrinking more than the laying. It is suspected that this is due to the interface between layers contains more polymer binder than ceramic powder, which makes these parts shrink further. Since the standing bar has more layers, this effect becomes more pronounced in this case.

4.7 Results Regarding the Component Density

A total of twenty-nine bending bars were tested for their density, all of them sintered in air at a temperature of 1450°C. Of these, twenty-one had been printed and debound in a standing manner and had no visible flaws when painted with a marker. The mean bulk density of these was 99.56% of the theoretical density. Five of the measured bending bars had been printed and debound in a laying fashion. These had a slightly higher bulk density, at 99.73% of the theoretical density. Of all the twenty-five bars, none of them showed a density below 99%. As such, the density itself appears to hold a high standard. In theory, if this high density can be maintained upon switching the powder or the polymer components in the suspension, then additive manufacturing of ceramic components using SL should be possible without compromising the material properties.

4.7.1 Impact of Sintering Temperature on the Density

The sintering temperature noticeably affected the final density. A selection of representative densities for the different bodies can be seen in table 3. Note that the bars have been printed, whereas the disks have been produced through conventional pressing.

Table 3: Measured densities for various sintering temperatures and components. A high temperature tended to give a higher density. The bars have been produced through printing, while the disks were made by pressing the powder.

Sintering Temperature (°C)	**Bar Density (% of theoretical)**	**Disk Density (% of theoretical)**
900	58,54	-
1300	98,70	95,37

1350	99,44	98,67
1400	99,60	99,69
1450	99,39	99,52
1500	99,52	99,95

For the lower temperatures, the bending bars tended to have a higher density than the conventionally produced disks, while at the higher sintering temperatures (1400-1500℃) the disks were a little better than the bending bars. This makes sense, as the disks were larger than the bending bars, and since sintering is dependent on diffusion, it likely takes them higher temperature/ longer time to reach full density, whereas the bending bars do so more readily. However, at the higher temperatures it can be assumed that both the disks and the bars have reached their maximum density, and by then the conventionally produced disks are a little bit better than the printed bending bars.

4.8 Results regarding the bend tests

A total of 83 bending bars were tested with a three-point bend test. However, the first twenty were made before the procedure had been honed to consistency. Furthermore, a three more proved to have defects so severe they could not be measured and are therefore not representative for the material performance. Hence 23 bars are omitted. The 59 remaining bars were arranged in groups of printing trays, so all bending bars in one group were part of the same tray. The group sizes differed depending on how successful the debinding process was for the given tray; often the group size was between four and eight bending bars. Across all 59 bending bars, the mean stress at break was determined to be 829 MPa, with the highest one measuring 1297 MPa. This, however, varied greatly between groups. A select few with a stress at break similar to the mean was selected and studied with an SEM, in an attempt to understand the reason for failure. An overview of the presented samples can be found in table 4.

Table 4: Details on the bending bars investigated with SEM. The stress at break is both above and below the mean value, with greater emphasis on breaks below it to understand those defects.

Test Number	**Force to Fracture (N)**	**Stress at Break (MPa)**
1	170	513
2	240	680
3	260	748
4	220	679
5	290	843
6	260	732

The defect causing the fracture could be found on all investigated bending bars. The defect sizes ranged from about 200µm to 10µm and to some degree correlated to the stress at break. Looking at the images 14 and 15 reveals that the defect size and defect position both are of utmost importance for the factor toughness of the material. Figure 14 shows the SEM-image of sample number one in table 4. It has a defect the size of about 50 µm located at the edge of the sample.

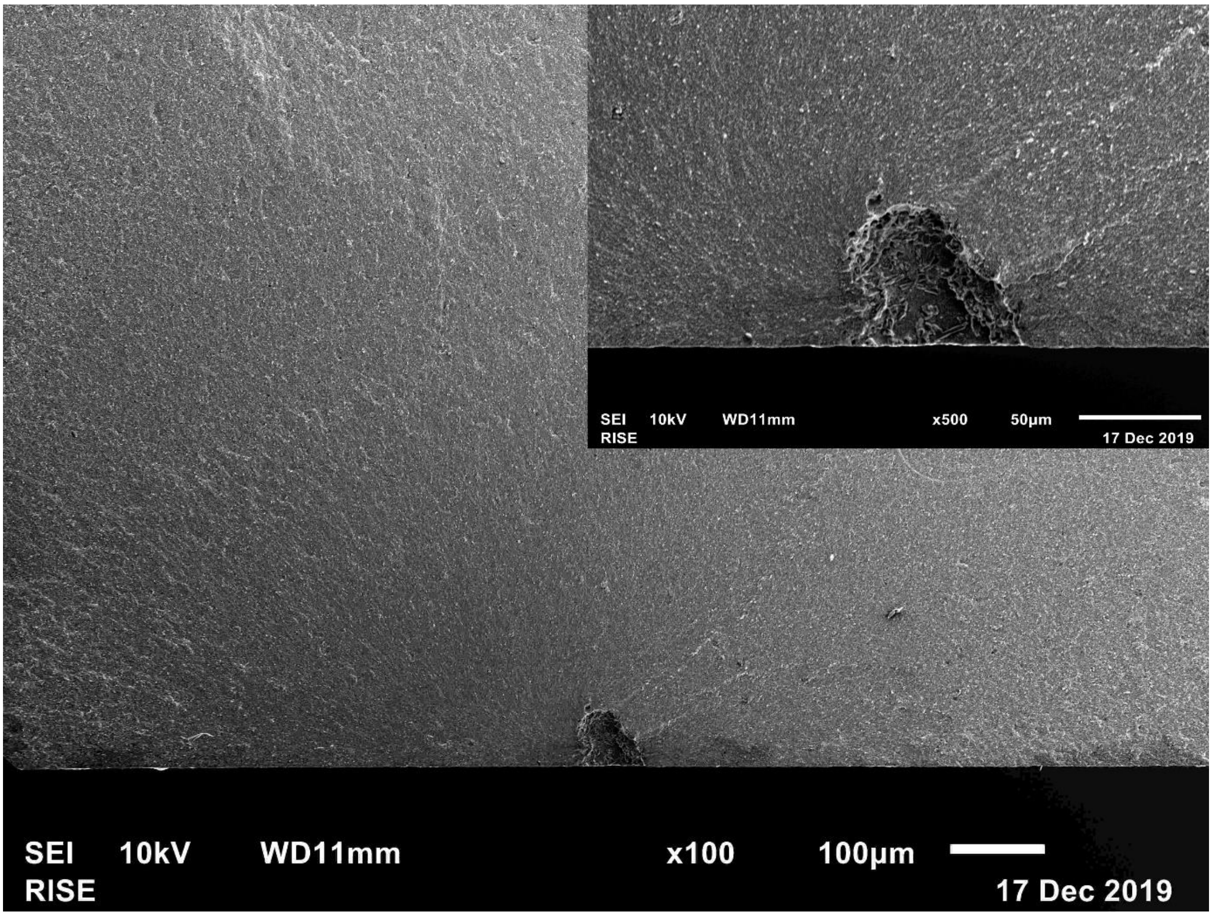

Figure 14: SEM-image of Bending Bar number 1 in table 4, with a stress at break of 513 MPa. The fracture defect is placed at the very edge of the sample and is about 50 µm across.

This can be compared to figure 15, which shows sample number two in the table. This sample had a better result on the stress at break (680 compared to 513). Yet, the images reveal that the defect causing the fracture was much larger in sample number three; about 150 µm at the widest point. However, since the defect was not located at the edge of the sample, the material nonetheless could survive a higher stress than bending bar number one.

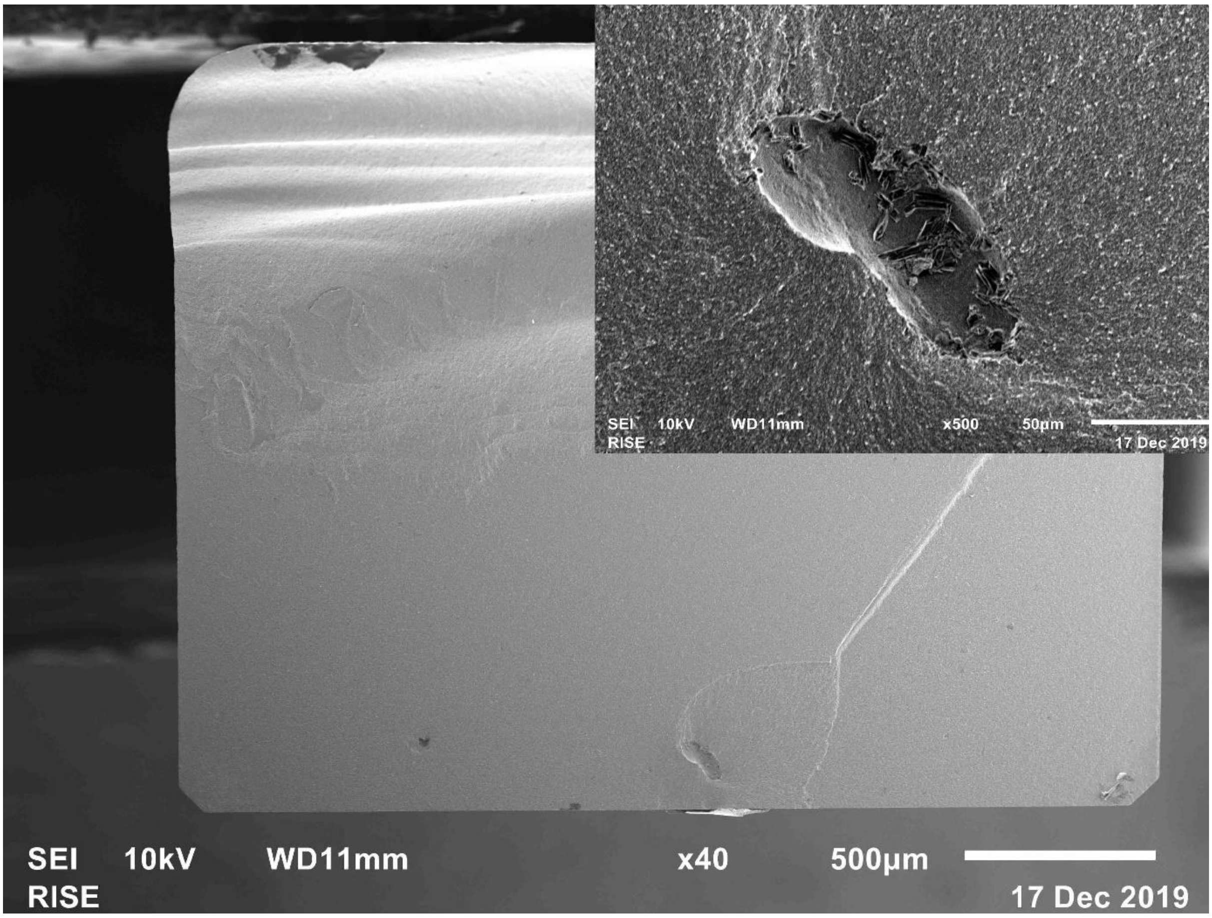

Figure 15: SEM-image of Bending Bar number 2 in table 4, with a stress at break of 680 MPa. The fracture defect is placed about 60 µm inside the sample from the lower edge, and is about 100 µm across if measured horizontally at the thickest point.

This conclusion can be further supported by studying figure 16, which is image of bending bar three. Much like bending bar two, this sample had a severe defect located in the middle of the sample; much larger than the one at bending bar two (more than 200 µm). However, this sample still claimed the second highest stress at break of the seven measured here. It is also located further from the edge than the defect in sample number two. The defects in both sample one and two looks rather similar. They are both appear rounded (if not perfectly spherical) hollows and are comparable in size. The defect in bar number three is significantly larger than the previous two and appears flatter than the others. It is suspected that defects like those present in sample two and three arise due to hard granules present in the powder, rather than as a result of the preparation or printing of the slurry. If so, perhaps the problem could be solved by more carefully mill and disperse the powder. The defect in bar number seven is less certain, but perhaps it can stem from imperfect breaking of agglomerates during the addition of the powder to the monomer mixture. Since it is so large, the hypothesis is that an agglomerate was present in the monomer mixture and then was crushed during the building process. If so then the issue should be rare and could be addressed by allowing for a longer or more aggressive mixing of the powder to the monomer mixture, as to ensure the powder is crushed to its smallest aggregates.

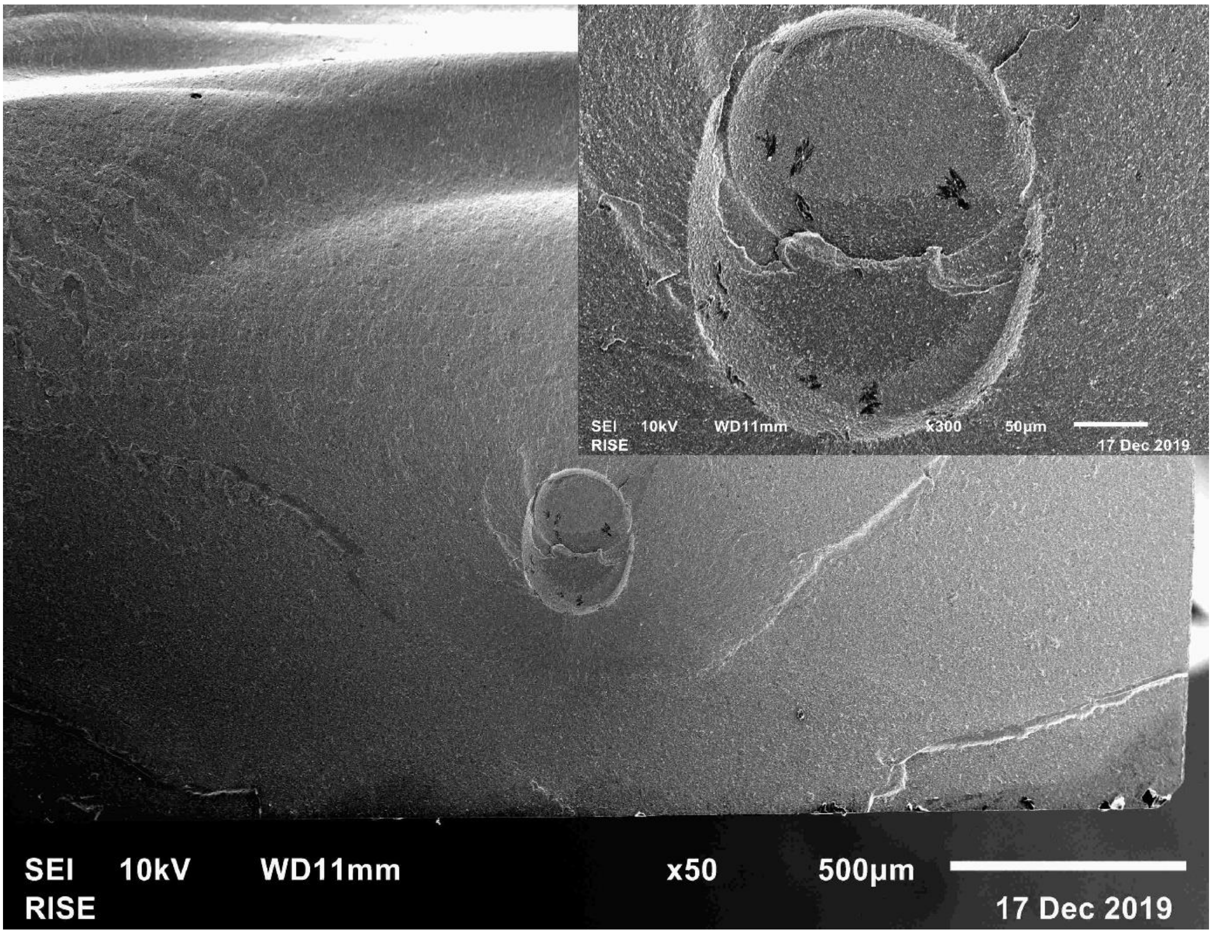

Figure 16: SEM-image of Bending Bar number 3 in table 4, with a stress at break of 748 MPa. The fracture defect is placed close to the middle of the sample and is about 200 µm across.

Notice in table 4 that samples number two and number four measure almost identical stress at break. The image of bending bar number four can be seen in figure 17. The defect is located at the edge. By comparing these two samples, it seems like a defect of 100 µm, located about 60 µm inside the sample is comparable to a defect of about 40 µm on the sample edge.

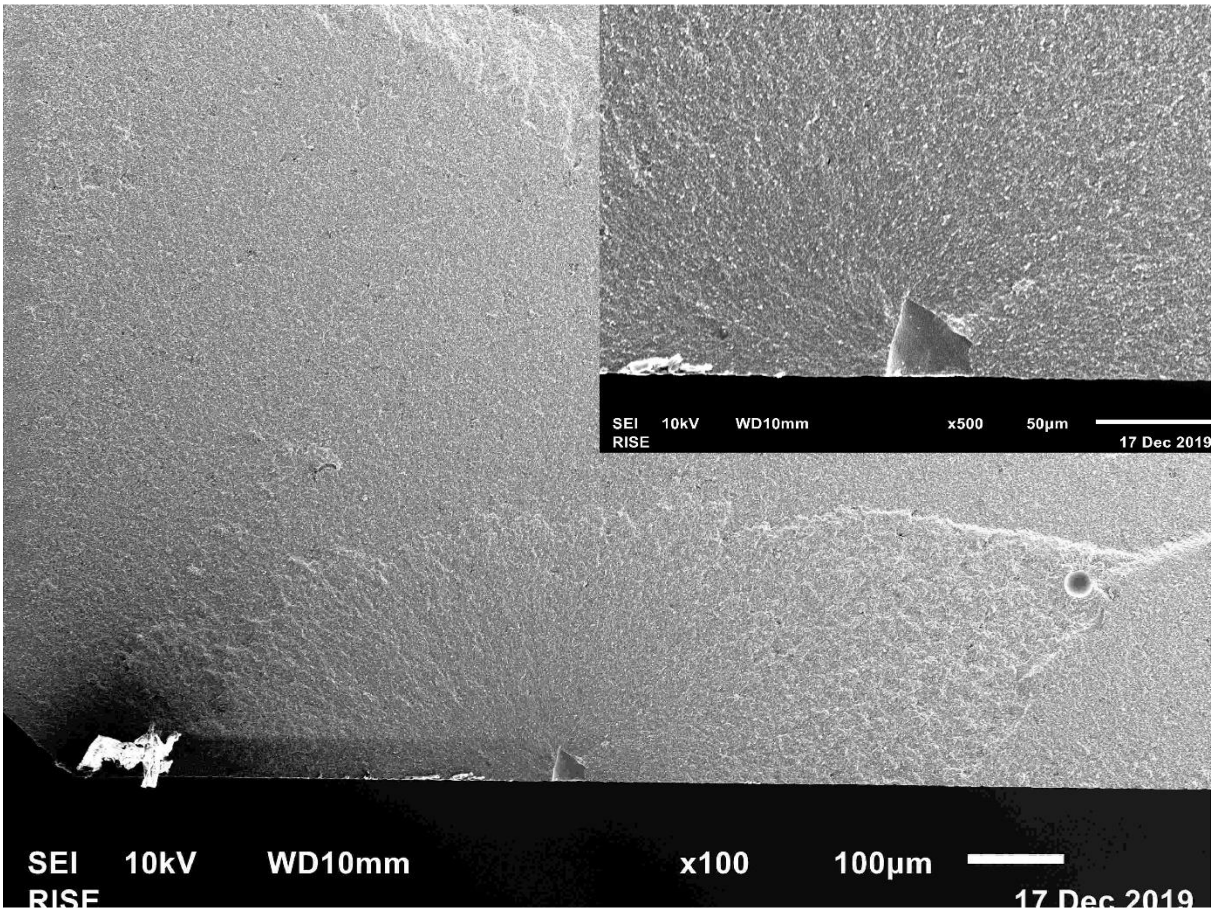

Figure 17: SEM-image of Bending Bar number 4 in table 4, with a stress at break of 679 MPa. The fracture defect is placed at the edge of the sample and is about 40 µm across. Notice the fracture mirror around the defect and the pore to the right of the image. The fracture mirror extends to include the pore as it represents a weakness in the material.

The defect depicted in figure 17 also differs from the defects in the previously discussed samples, as it appears to be a splinter missing from the sample, rather than a round lump of material. How this defect occurred is unknown, but it might be due to careless handing at some stage of the production chain. It appears to be a mechanical damage rather than something that stems from the powder itself. Likewise, it seems unlikely that the printing or debinding would result in a defect of this nature.

Bending bar number five measured the highest stress at break of these seven samples. The corresponding SEM image can be found in figure 18.

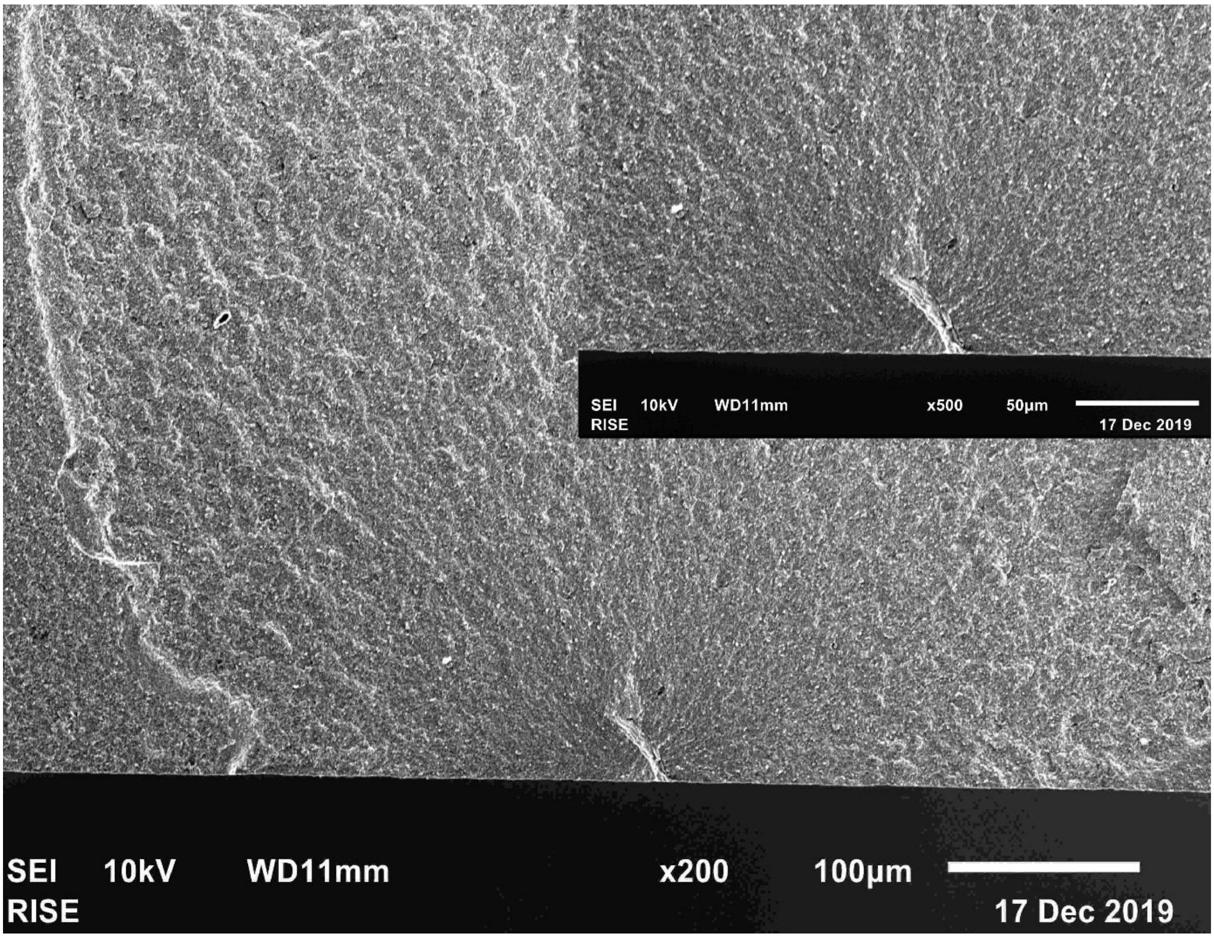

Figure 18: SEM-image of Bending Bar number 5 in table 4, with a stress at break of 843 MPa. The fracture defect is placed at the edge of the sample and is about 10 µm horizontally across. The defect most likely occurred due to the inclusion of an errant fiber being included in the printing suspension.

Initially, this defect, much like the one in sample number five, does not seem to be due to an agglomerate like in samples two and three, as this one is not rounded and smaller than those. However, comparison with the defect in bending bar six, displayed in figure 19 reveals that this defect too seems to be due to imperfections in the powder. figure 19 reveals a long, arching defect. Since the bottom parts of the bending bars are ground, it is suspected that the defect present in figure 18 is of the same type that is present in figure 19, only with most of the defect ground away. In figure 19, the defect seems to stem from another granule that has partially integrated with the surrounding ceramic but left an interface where the former granule met the homogenous powder. Most likely this arose due to the shrinkage during debinding, as the granule shrunk at a different speed compared to the surrounding material and hence caused interior stress along the interface.

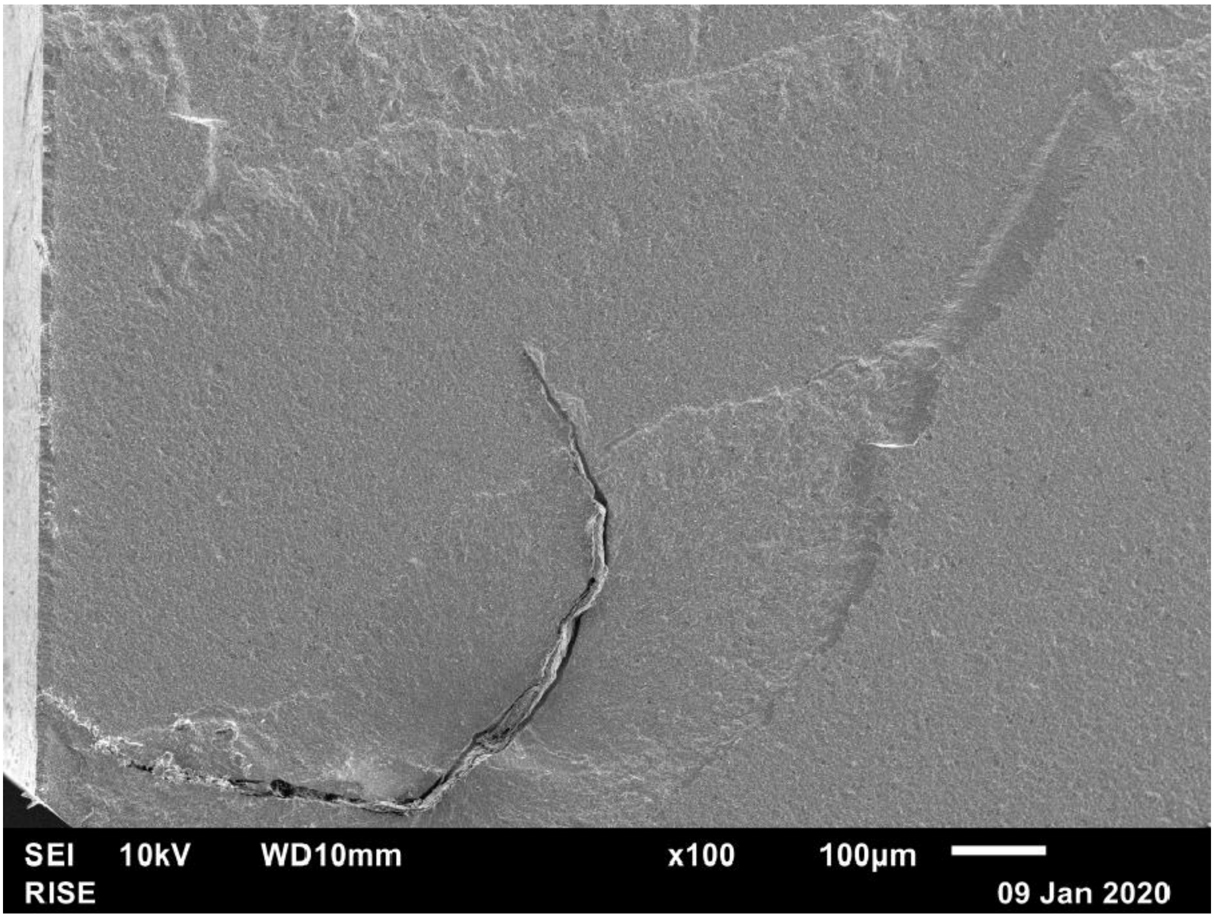

Figure 19: SEM-image of Bending Bar number 6 in table 4, with a stress at break of 732 MPa. The fracture It is suspected to be the same type of defect as seen in figure 18, only the one in figure 18 had been ground away when preparing the bending bar.

One of the most successful groups consisted of eight bending bars. The measured results are presented in table 5.

Table 5 Results from one of the most successful groups of bending bars. Notice bar number six failing much earlier than the others.

Bending Bar Number	**Force to Fracture (N)**	**Stress at Break (MPa)**
1	**330**	**990**
2	**300**	**820**
3	**450**	**1246**
4	**320**	**919**
5	**370**	**1081**
6	**60**	**153**
7	**420**	**1180**

Of these seven, one stands out. Bending bar number six failed significantly earlier than the others and was investigated with the SEM. The pictures are presented in figure 20 and figure 21.

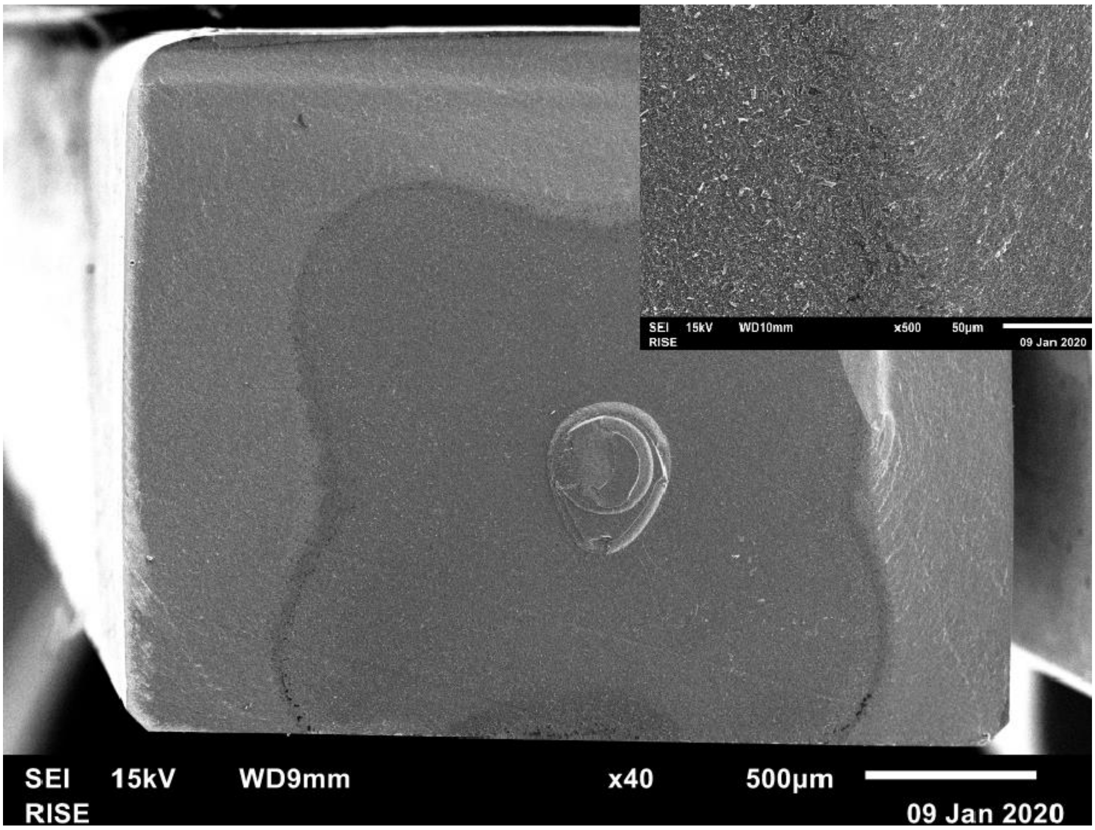

Figure 20: Cross section of the weakest bending bar in the most successful group. Notice the darkened surface around the middle defect. The small photo is of the interface between the two surfaces (darkened surface to the left).

Two different types of surfaces can be seen in figure 20. Most of the edges have a surface like any other bending bar. Between the center of the bending bar and the edge there is another, darker surface.

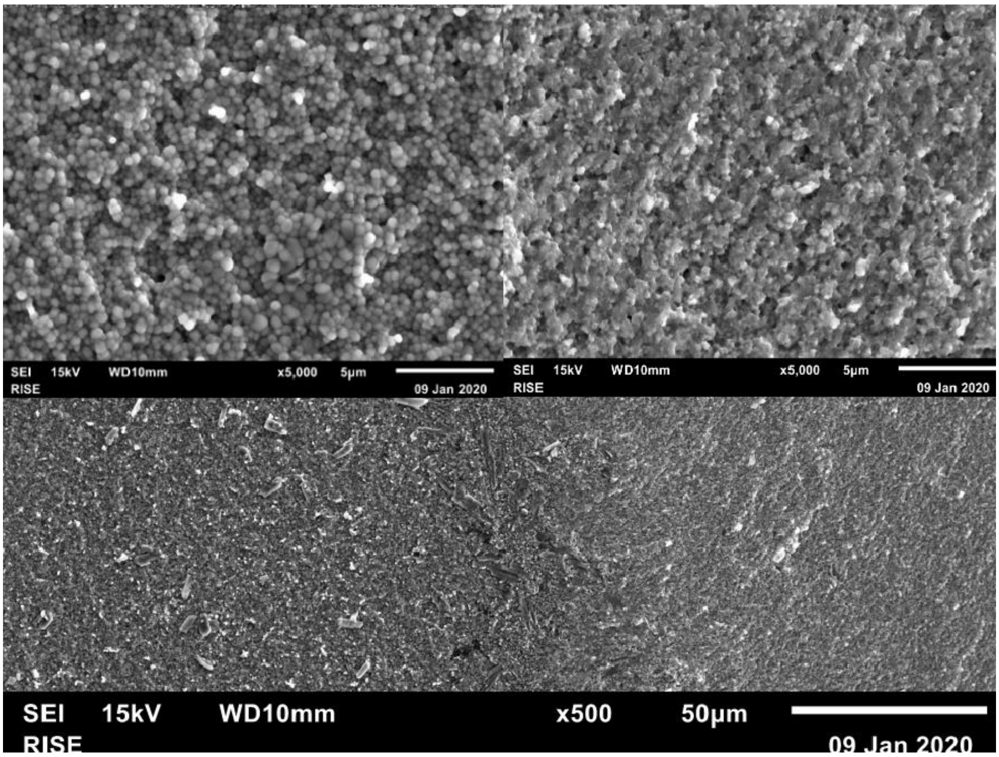

Figure 21: Cross section of the weakest bending bar in the most successful group. A comparison between the dark, unsintered surface (upper left), the sintered surface (upper right) and the interface between the surfaces (lower image)

Upon magnifying the two surfaces, further differences can easily be seen (in figure 21). The surface around the edge is rough and possesses clear ridges stemming from the break of the bending bar. Individual grains cannot be seen clearly. All this point towards this area having been sintered successfully. The other surface, however, clearly lacks the ridges associated with a cracked surface, and is made up by clearly visible individual grains. This means that these grains have not been sintered to other grains. Instead, they have adopted the spherical form to minimize their own surface area. This means that the darker surface in the middle of the bending bar never was connected to another surface but delaminated and formed a cavity in the middle of the bending bar, leading to the severely reduced stress resilience. The middle of the bending bar reveals a crushed granule like the one seen in figure 16. This is thought to be the reason for the formation of the cavity by reducing the adhesion between the two layers around it.
The mean stress at break in this series of bending bars is 892,13 MPa, but due to the massive defect in bending bar number six not stemming from the material itself but a failure in the printing process, it should be discarded from an investigation of the material properties. Excluding bending bar number six yields a mean stress at break of 998 MPa.

4.8.1 Weibull Modulus

The Weibull modulus across all experiments is 1,96, which indicates that the material does not show a very uniform stress tolerance. Arranging the bending bars in order of increasing toughness and plotting it against the respective probability of failure yields the curve depicted in figure 22.

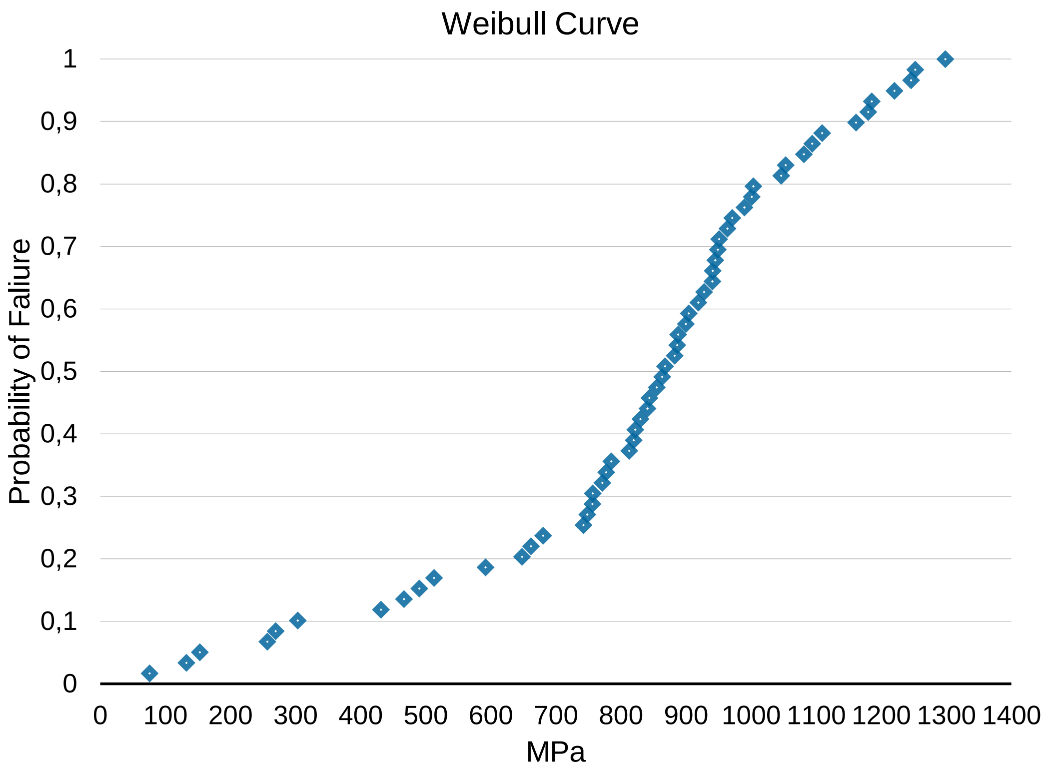

Figure 22 sample strength against Probability of Failure. A few distinct regions with some internal linearity can be seen. The lowest measurements, (0-700 MPa) falls on a rough line, the values between 700-1000 MPa follow another, steeper line and the strongest samples (+1000MPa) follow another line.

Looking at the curve, three distinct regimens can be seen. The lower values (0- 700 MPa) seem to fall only on one line, whereas the intermediate values (700-1000 MPa) seem to fall on another, steeper curve. The very highest values finally seem to fall on yet another line. The different Weibull moduli for these three curves were calculated to 1.18 for the lowest measurements, 5.24 for the intermediate measurements and 0.96 for the highest measurements. This indicates that there are three different types of defects that are present in this material, each type responding to a certain toughness interval. Based on the discussion about the SEM images in section 4.8, it seems that the bending bars in the lowest regimen (0-700 MPa) tend to have defects most often deriving from imperfections in the powder, with hardened agglomerates of varying sizes that cause the defect responsible for fracture. However, given the low Weibull modulus of these samples, it appears that these defects are not uniform, but is subject to variance between different samples.

The intermediate regimen (700-1000 MPa) has a considerably higher Weibull modulus of 5.24. This indicates that these samples behave similarly, and it can be assumed that the defects causing the fractures in this interval are relatively similar. However, these samples have not been investigated with the SEM, as the lower regimen was considered more important to understand due to the detrimental nature of these defects. The exact nature of the defects in the intermediate regimen is therefore unknown.

The highest measuring bending bars have an even smaller Weibull modulus than the lower regimen at 0.96. This indicates a severe randomization of these defects. However, at these stress levels, the defects causing the fractures will be extremely small. It can be assumed that these miniscule defects are more or less unique to each sample, which would explain the low Weibull modulus.

4.9 Results Regarding Resolution and Angle Tests

The angles measured ranged from 0° to 90° relative to the samples standing on the printing pane with 0° being both the layer in direct contact with the printing pane, and the topside of the printed object. This means there are two of each angle, but they indicate different parts of the printed piece, as indicated by figure 26.

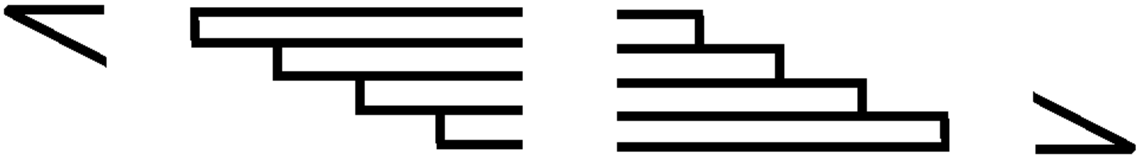

Figure 26: Both these sides are the same angle when measured from their respective reference plane, but they are different sides, one at the top and the other at the bottom of the printed object.

Every angle was measured at three different places and a mean Sa number was plotted for all these angles, as can be seen in figure 27.

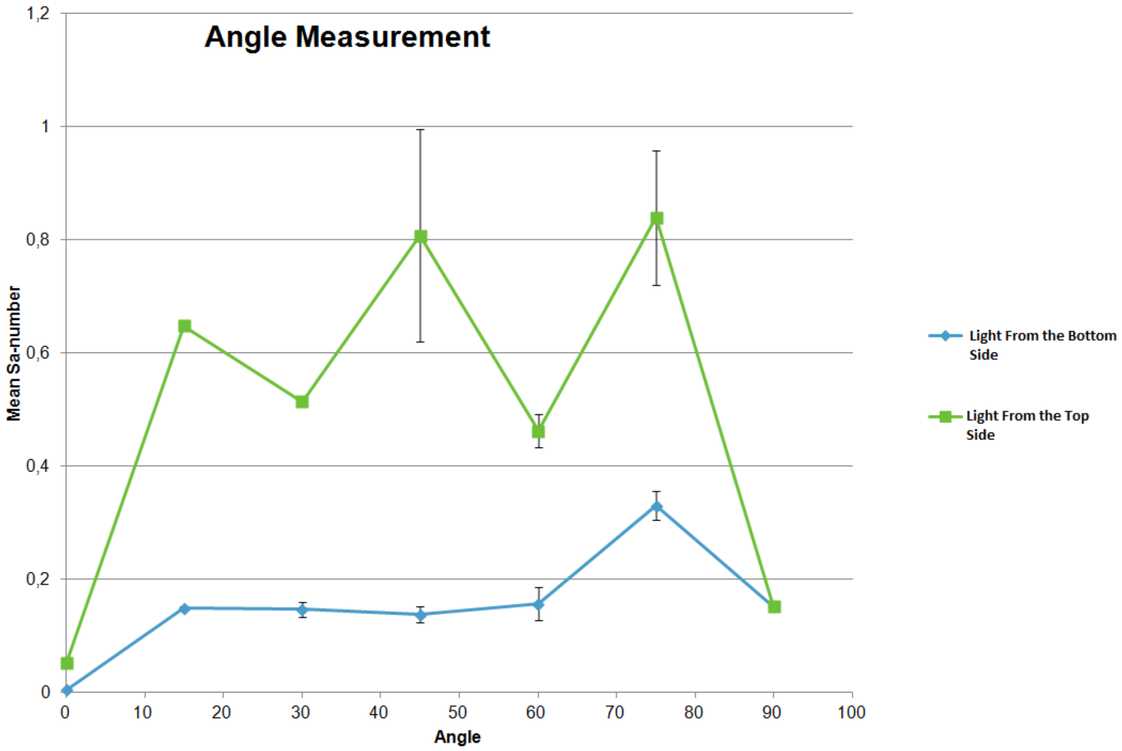

Figure 24: Plot of the mean Sa-numbers and their corresponding angle. There is a sharp increase in surface roughness upon the light coming from above, rather than below.

There is a clear distinction between the top and bottom parts of the printed objects. This is assumed to be because at the bottom side, every new layer printed is a little bit longer than the one before it. Due to this, the polymerization incurs a slight curvature of the slurry at the edge, due to the light intensity being stronger than what is needed for the layer to print (in order to get a good adhesion between the layers) there will be a slight curvature to the topmost part of these layers. See figure 25. Normally, the layer thickness set in the printer is 25 µm, but the cure exposure time would result in a layer of about a 100 µm thick.

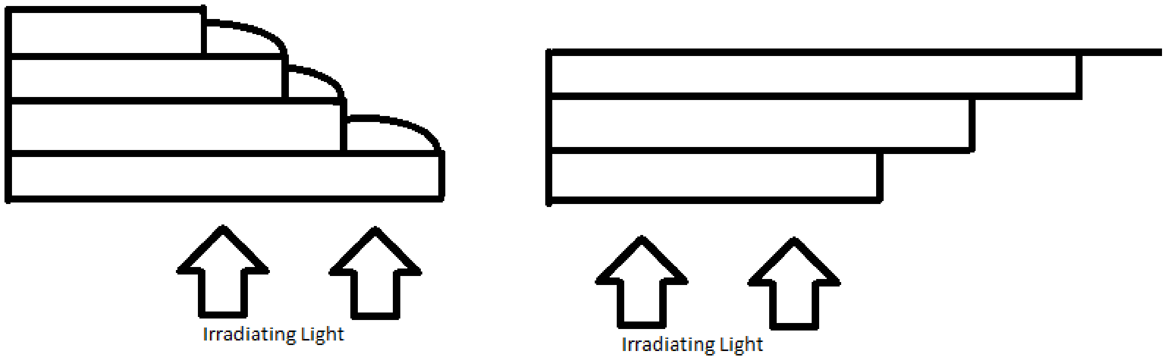

Figure 25. Pictographic representation of why the light coming from above impacts the surface roughness. The left picture gains a smoother finish as the light irradiates a little extraneous suspension above the protruding layers. This cannot happen in the rightmost picture.

This curvature results in these angles becoming smoother than they ought to be. However, on the topside this effect is no longer present as every layer now is a little bit shorter than the one above. Here the side of the printed goods looks like the side of a stair; every layer sharply pronounced, which leads to the high increase in Sa numbers for these angles. There is also the question of the sharp increase in Sa number at 75° on the bottom side. It is preceded with a minor increase in roughness at the angle before it (60°), so perhaps the roughness increases at angles above 45°. This should be verified by further measurements at intermediate angles, for example 65° and 70°. Furthermore, the Sa numbers for the topside at the angles 45° and 75° are significantly less stable than the for the surrounding angles. Most likely this is due to random chance, as the different measurements are less unanimous at these angles, and so the mean values become more scattered.

4.10 Results Regarding Printing Different Sized Components Using Suspension 3-33

The results regarding the printing of thicker components using suspension 3-33 are somewhat inconclusive. The experiment with short, bending bars of different thickness was repeated twice, both times with three bars of each thickness. The first time the result showed a clear progression of thicker bending bars being harder to debind. The thinnest bars (8X32X32 mm) were flawless, the second thinnest bars (8X42X42 mm) has one horizontal crack at about halfway up. The second thickest bars (8X52X52 mm) had more horizontal cracks as well as a few vertical cracks, running across the printed layers. Finally, the thickest bars (8X62X62 mm) had severe cracks in multiple lairs as well as prominent vertical cracks. However, when this experiment was repeated, all but the thickest bars all were flawless, and the thickest bars only showed a few horizontal cracks. One of the thickest bars even showed no cracks at all. Similar inconclusive results were obtained from the scaled-up versions of the bending bars. These were printed in a vertical fashion over the course of two days. One of them showed certain cracking but considering the size bars this was still relatively rare. There were no vertical cracks. However, upon repeating this experiment with an even longer debinding script, the bending bar showed a more severe cracking, including vertical cracks. The progression can be seen in figure 26.

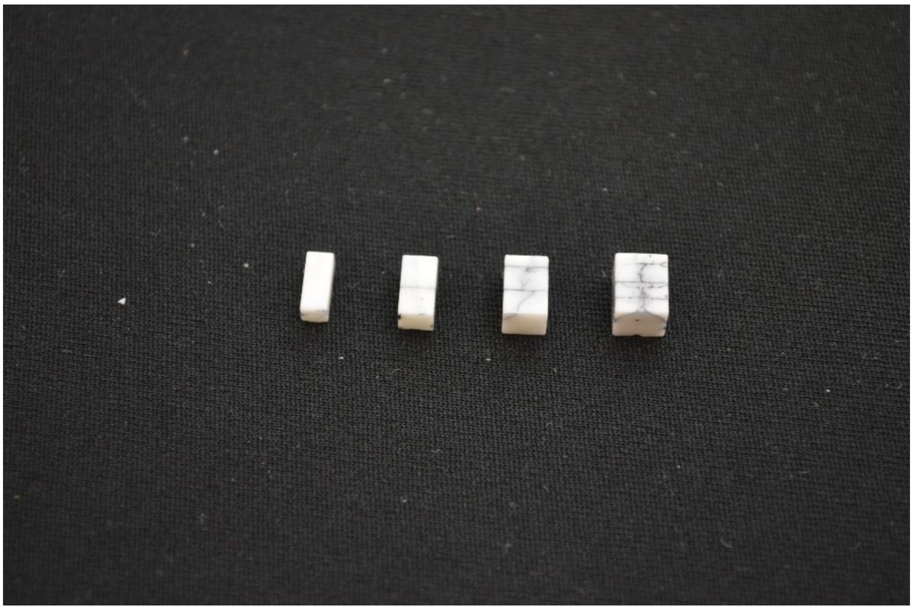

Figure 26: Progressively more severe defects of printed bending bars of different thicknesses.

4.11 Results regarding printing different sized components using suspension Exp-33

A hollow cylinder with a wall thickness of 4 mm and an in inner hole with a diameter of 4mm could be debound and sintered with relative success using suspension Exp-33. It was not flawless, as there were minor, horizontal cracks in the structure, but the cylinder could be stepped on without any further damage. The experiment was repeated with a similar hollow cylinder, using a slightly longer debinding script. This two showed one long, vertical on opposite ends, cracking the structure in two. However, this is thought to be due to a roughness on the plate on which the structure was debound, combined with the weight of the structure, which together prevented it to shrink unhindered. As such, further experiments must be conducted before the repeatability can be evaluated.

5.

Conclusions

It has been shown that in order to produce functional ceramic goods with a reasonable density using the SL technology, the debinding script and the monomer-powder suspension are both of utmost importance. However, the debinding script seems to be the more sensitive component. The suspension must be printable, but that is generally not hard to accomplish. The debinding script however depends heavily on the mixture itself, as well as the geometry of the individual printed component, and the results have been shown to vary between attempts, using the same suspension. Nevertheless, the script presented above have yielded useful results with general consistence. As revealed by the shrinkage and debinding experiments, the temperature range between 150 and 300 degrees is the most important for the debinding script, as that is when most of the polymer is burnt away.

Of the two monomer mixtures, 3-33 have shown decent success at producing bending bars that could be evaluated in a three-point bend test with a mean result of 829 MPa, across 59 bars. While there were always bending bars that failed to be successfully debound, the good results have been reproducible. The alternative suspension, Exp-33, has never quite succeeded in making flawless components like 3-33 did. However, for bulky pieces, the flaws produced using Exp-33 were significantly less severe than for 3-33. Exp-33 should therefore be developed further. However, the results it produced seems to indicate that it has potential.

5.1 Future works

From a material performance standpoint, the mean value is relatively high, and the very best samples show great promise. However, there are still plenty of defects present in the samples that seems to stem from impurities in the powder. Further investigations in how the powder should be handled to remove these imperfections would be a significant improvement. Potentially this could increase the mean value, as well as improve the Weibull modulus, which is currently badly affected by the weaker samples.

To further develop the study of the printed surface, a first test would be to test the bending bars directly in the bend test, rather than grind one side down. This will investigate the frequency, size, and nature of the defects arising from the printing process itself, rather than the material performance.

The debinding process works reasonably well, but there are still plenty of bending bars that has to be rejected from every tray. Further development is needed to make the printing process more consistent. As such, further developments to the debinding script should be considered, varying the different temperatures and hold times.

References

[1] C. Barry Carter, M. Grant Norton, *Ceramic Materials: Science and Engineering*, Springer, 2007, pages 1-12

[2] E. Medvedovski, *Wear Resistant Engineering Ceramics*, Wear, 2001, Vol 249, pages 821-828

[3] D.W. Richerson, W.E. Lee, *Modern Ceramics Engineering; Properties, Processing and Use in Design, fourth edition*, CRC Press, 2018, Pages 203-268, 523-575

[4] A. Ghazanfari, W. Li, M.C. Leu, J.L.Watts, G. E. Hilmas, *Additive manufacturing and mechanical characterization of high density fully stabilized zirconia*, Ceramics International, 2017, vol. 43, pages 6082-6088

[5] P. Francesco M. Pierfrancesco R. Iommetti L. Raffaelli, *An overview of zirconia ceramics: Basic properties and clinical applications*, Journal of Dentistry, 2007, Vol. 35, pages 819-826

[6] S.C. Singhal, *Advances in solid oxide fuel cell technology*, Solid State Ionics, 2000, vol. 135, pages 305-313

[7] M. Boaro, Aricó A. S. *Advances in Medium and High Temperature Solid Oxide Fuel Cell Technology*, CISM International Center forMechanical Sciences, Vol. 574, Springer 2017

[8] Z. Chen, Z. Li, J. Li, C. Liu, C. Lao, Y. Fu, C. Liu, Y. Li, P. Wang, Y. He, *3D printing of ceramics: A review*, Journal of the European Ceramic Society, 2019, vol. 39, pages 661-687

[9] K. V. Wong, A. Hernandez, *A Review of Additive Manufacturing*, International Scholarly Research Network, 2012

[10] A.G. Evans, R.M. Cannon, *Overview no. 48: Toughening of brittle solids by martensitic transformations*, Acta Metallurgica, 1986, Vol. 34 Pages 761-800.

[11] Formlabs, The Ultimate Guide to Stereolithography (SLA) 3D Printing, site updated 2019, site retrieved 2019-09-09, https://formlabs.com/blog/ultimate-guide-to-stereolithography-sla-3d-printing/#sla-systems

[12] C. Piconi, A.A. Porporati, *Bioinert Ceramics: Zirconia and Alumina*, Handbook of Bioceramics and Biocomposites, Springer, 2015, Pages 1-25.

[13] R. Kelly, I. Dendry, *Stabilized zirconia as a structural ceramic: An overview*, Dental Materials, 2008, Vol.24, Pages 289-298.

[14] J.F. Shackelford, R.H Doremus, Ceramic and Glass Materials, Springer, 2008, Pages 169-198.

[15] R.C. Garvie, R.H. Hannink, R.T. Pascoe, *Ceramic Steel?*, Nature, 258, 1975, Pages 703-704

[16] G. Y. Akimov, E. V. Chaika, G. A. Marinin, *Wear and Fracture Toughness of Partially Stabilized Zirconia Ceramics under Dry Friction Against Steel*, Journal of Friction and Wear, 2009, Vol. 30, Pages 77-79.

[17] R. Morrell, *Ceramics, Structural*, Kirk-Othmer Encyclopedia of Chemical Technology, John Wiley& Sons Inc. 2011.

[18] G.A.L Peñaloza, *Additive Manufacturing of Zirconia; Master's thesis in Materials Engineering*, Chalmers University of Technology, 2018

[19] Tosoh Corperation, Products, Zirconia Powders, retrieved 2019-09-18 https://www.tosoh.com/our-products/advanced-materials/zirconia-powders

[20] M. Bengisu, *Engineering Ceramics*, Springer, 2001, Pages 356-360

[21] H. Xie, S. Shen, M. Qian, F. Zhang, C. Chen, F. R. Tay, *Effects of Acid Treatment on Dental Zirconia: An In Vitro Study,* PLOS one, 2015.

[22] A. Scarano, F. Di Carlo, M. Quaranta, A. Piattelli, *Bone response to zirconia ceramic implants: an experimental study in rabbits*, PubMed, Vol XXIX, 2003

[23] M. Hasegawa, A. Sudo, *In vivo wear performance of highly cross-linked polyethylene vs. yttria stabilized zirconia and alumina stabilized zirconia at a mean seven-year follow-up*, BMC Musculoskeletal Disorders, 2013, Vol. 14.

[24] C. Oblak, I. Verdenik, M.V. Swain, T. Kosmac, *Survival-rate analysis of surface treated dental zirconia (Y-TZP) ceramics*, Journal of Materials Science: Materials in Medicine, 2014, Vol.25, Pages 2255-2264

[25] M.J. Verkerk, A.J.A. Winnubst, A.J. Burggraaf, *Effects of impurities on sintering and conductivity of yttria-stabilized zirconia*, Journal of Materials Science, 1982, Vol.17, Pages 3113-3122

[26] O. Lyckfeldt, M. Sjöstedt, J. Orlenius, *Freeze Granulation Product Sheet*, Swerea IVF

[27] Lithoz, *Additive Manufacturing Systems for ceramics*, Site retrieved 31/10-19, https://www.lithoz.com/en/our-products/am-systems

[28] P.J. Bártolo, *Stereolithography: Materials, Processes and Applications*, Springer, 2011, Pages 12-20, 37-56, 81-112

[29] C. Montanari, *Additive Manufacturing of Silicon Nitride*, Luleå University of Technology, 2017.

[30] Polymer Properties Database, CROW Polymer Science , 2015, retrieved 2019-10-30, https://polymerdatabase.com/polymer%20chemistry/Photoinitiators1.html

[31] M. Wen, L. Voon, J.A. Payne, L.F. Francis, L.E. Scriven, A.V. McCormick, *Kinetic Study of Free-Radical Polymerization of Multifunctional Acrylates and Methacrylates*, IS&T, copyright 1997.

[32] M.L. Griffith, J.W. Halloran, *Freeform Fabrication of Ceramics via Stereolithography,* Journal of the Maerican Ceramic Society, 1996, Vol. 79, Pages 2061-2608

[33] C. Bae, J. Halloran, *Influence of Residual Monomer on Cracking in Ceramics Fabricated by Stereolithography*, International Journal of Applied Ceramic Technology, 2011, Vol. 8, Pages 1289-1295.

[34] W. Harrer, M. Schwentenwein, T. Lube, R. Danzer, *Fractography of zirconia-specimens made using additive manufacturing (LCM) technology*, Journal of the European Ceramic Society, 2017, Vol.37, Pages 4331-4338.

[35] W.M. Ahmed, T. Troczynski, A.P. McCullagh, C.C.L. Wyatt, R.M. Carvalho, *The influence of altering sintering protocols on the optical and mechanical properties of zirconia: A review.* Journal of Esthetic and Restorative Dentistry, 2019, Vol. 31 Pages 423–430

[36] B. Stawarczyk, M. Özcan, L. Hallmann, A. Ender, A. Mehl, C. H. F. Hämmerlet, *The effect of zirconia sintering temperature on flexural strength, grain size, and contrast ratio*, Clinical Oral Investigations, 2013, Vol. 17, Pages 269-274

[37] j. Schmit, A. Pakuła, White Light Interferometry,Handbook of Advanced Non-Destructive Evaluation, Springer, 2018, Pages 1-47

[38] W.J. Walker Jr, J.S. Reed, *Influence of Granule Character on Strength and Weibull Modulus of Sintered Alumina*, Journal of American Ceramic Society, 1999, Vol. 82, Pages 50-56